Development of mean-field continuum dislocation kinematics with junction reactions using de Rham currents and graph theory

Kyle Starkey[1 a], Thomas Hochrainer[b], Anter El-Azab[a]

[a] *School of Materials Engineering, Purdue University, West Lafayette, IN 47907, USA*
[b] *Institut für Festigkeitslehre, Technische Universität Graz, Kopernikusgasse 24, 8010 Graz, Austria*

Abstract

An accurate description of the evolution of dislocation networks is an essential part of discrete and continuum dislocation dynamics models. These networks evolve by motion of the dislocation lines and by forming junctions between these lines via cross slip, annihilation and junction reactions. In this work, we introduce these dislocation reactions into continuum dislocation models using the theory of de Rham currents. We introduce dislocations on each slip system as potentially open lines whose boundaries are associated with junction points and, therefore, still create a network of collectively closed lines that satisfy the classical relations $\boldsymbol{\alpha} = \mathrm{curl}\boldsymbol{\beta}^{\mathrm{p}}$ and $\mathrm{div}\boldsymbol{\alpha} = 0$ for the dislocation density tensor $\boldsymbol{\alpha}$ and the plastic distortion $\boldsymbol{\beta}^{p}$. To ensure this, we leverage Frank's second rule at the junction nodes and the concept of virtual dislocation segments. We introduce the junction point density as a new state variable that represents the distribution of junction points within the crystal containing the dislocation network. Adding this information requires knowledge of the global structure of the dislocation network, which we obtain from its representation as a graph. We derive transport relations for the dislocation line density on each slip system in the crystal, which now includes a term that corresponds to the motion of junction points. We also derive the transport relations for junction points, which include source terms that reflect the topology changes of the dislocation network due to junction formation.

1. Introduction

The present work introduces a new paradigm for incorporating dislocation junction reactions in continuum dislocation dynamics modeling of mesocale plasticity. The development of plasticity theories using continuum descriptions of dislocations has received much attention in the mathematics, mechanics, and materials science communities for many decades (Kröner, 2001; Deng and El-Azab, 2007; Hochrainer et al., 2007; Groma, 1997). It is known that the treatment of dislocations within a continuum or density-based framework presents a major challenge, not least because they react to form complex three-dimensional networks Sills et al. (2016). Dislocation reactions include cross slip, a process by which a moving dislocation line changes its glide plane, annihilation reactions, and junction formation. Such processes are responsible for the dislocation multiplication, immobilization of a significant part of the

[1] Corresponding author.

dislocation population, and the subsequent emergence of self-organized dislocation density patterns (Bulatov and Cai, 2006). A junction reaction is one in which two dislocation segments with different Burgers vectors react to form a segment of a third Burgers vector, which may be mobile in the crystal (glissile junction), immobile (sessile junction), or null (annihilation).

Junction formation has received a great deal of attention in discrete dislocation dynamics models (Madec et al., 2002; Sills et al., 2018). Many authors have also investigated the strength of these junctions using atomic scale models (Rodney and Phillips, 1999; Martínez et al., 2008; Zbib et al., 2000; Shenoy et al., 2000). In discrete dislocation dynamics, it has been shown that among the various types of junctions reactions, glissile junctions are one of the main contributors to hardening because they lead to dislocation multiplication (Sills et al., 2016). Sessile junctions, on the other hand, are believed to anchor the dislocation pattern and lead to its refinement. Currently, the literature on discrete dislocation dynamics has abundant information describing the topology of dislocation networks including junctions. This information comes in the form of the connectivity information between the lines and nodes in the dislocation network (Po et al., 2014), which is updated as the network evolves under applied stress. While the discrete dislocation dynamics models easily track dislocation networks in 3D by introducing rules for cross slip and junction formation, continuum dislocation dynamics formulations are still lacking such a representation as they mostly rely on the average line length information, see, for example, Stricker and Weygand (2015), Starkey et al. (2020), Arora and Acharya (2020), and Hochrainer (2016).

Continuum dislocation dynamics (CDD) theories which incorporate long range interactions in microscopic driving forces (resolved shear stresses) have been derived from pair correlations for strongly simplified systems of straight parallel edge dislocation (Groma, 1997; Groma et al., 2003; Ispánovity et al., 2020). Continuum variables suited to characterize systems of curved dislocation lines have been introduced, which may be combined with standard methods of irreversible thermodynamics to obtain natural generalizations of the quasi-2D theory of straight edge dislocations (Hochrainer, 2016). However, the continuum theory of curved dislocations currently lacks the consideration of dislocation junctions and other dislocation reactions, which are known to cause the emergence of a yield stress and its evolution in strain hardening, a process that is attributed to the multiplication of dislocations. Various dislocation reactions and dislocation multiplication have been recently incorporated in continuum theories of dislocations, both in the so-called line-bundle approximation (Lin and El-Azab, 2020) and in the higher length scale CDD theory (Monavari and Zaiser, 2018; Stricker et al., 2018; Sudmanns et al., 2019). The available models for dislocation reactions and junctions are usually adopted from empirical rules and are based on statistical dislocation variables, which do not reflect the complex interconnected network formed by dislocations. Ideally, if the dislocation density variables would reflect the salient features of the dislocation networks, their evolution should 'naturally' account for reactions and multiplication. However, so far, no continuum variables have been suggested which would reflect at least in a rudimentary way the complexity of an interconnected network of dislocations.

As of now, the most detailed way of describing the dislocation content of a volume element in CDD is a series of dislocation alignment and curvature tensors (Hochrainer, 2015; Weger et al., 2021) which approximate a higher

dimensional vectorial description of closed dislocation lines (Hochrainer, 2007). Differential forms have been an important tool for the development of the higher dimensional theory, which are obtained from averaging dislocations viewed as (vector valued and higher dimensional) de Rham currents (Hochrainer, 2007). Also the named tensor series may be obtained from averaging tensor valued de Rham currents. In an n-dimensional space, smooth differential $(n-1)$ forms may represent densities of curves and thus in principle also curves which make up a complex network. However, while the notion of closeness of differential forms comprises some topological information, most of the topology of the network is not reflected in such differential forms; the topology of networks falls in the realm of graph theory but the graph theory itself does not describe the geometry of the dislocation network.

In the current work, we take first steps to integrate dislocation network information, including dislocation junctions and their connections to adjacent lines, into a continuum description of dislocations. In doing so, we use a vector representation of the dislocation density within the line bundle approximation, where the density on a given slip system has a single line direction at every 'continuum' point in space. Within this framework, the resolution is selected such that the geometric cancellation due to the use of a vector representation of the density coincides with the physical annihilation of dislocations (Vivekanandan et al., 2021; Anderson and El-Azab, 2021). An important tool to be used regard to developing a continuum description of dislocations is de Rham integral currents (de Rham, 1984), where we consider dislocation networks to consist of junction points and line like interconnects. The connectivity information of the dislocation network is established by using the graph theory. In doing so, we exploit the partitioning characteristics of dislocation networks which result from the nature of the junction formation process, specifically the induced subgraphs corresponding to each type of junction. Focusing mainly on glissile junction representation in continuum dislocation dynamics, we introduce a junction point density to model the evolving dislocation network. The introduction of this density amounts to building connectivity information into the continuum dislocation dynamics framework.

In the next section, we introduce some of the mathematical preliminaries, including de Rham integral currents. The following section introduces the dislocation density tensor on each slip system for the case in which dislocations may be open or closed lines due to reactions. We show that, due to Frank's second rule the total dislocation density tensor and plastic distortion still satisfy $\int_F \boldsymbol{\alpha} = \int_{\partial F} \boldsymbol{\beta}^p$. In the next section, we introduce a new object, $\boldsymbol{\Pi}^{(l)}$, which is a measure of the endpoints of dislocation lines of each slip system l. We show that this new measure is related to the dislocation density tensor on the lth slip system, through $\boldsymbol{\Pi}^{(l)} = \mathrm{d}\boldsymbol{\alpha}^{(l)}$. We then represent the dislocation network in a graph-theoretic setting in order to establish a connection between the endpoint density and the junction point density for one junction type. While establishing this connection, we found that, for the case of dislocation networks established via glissile junction formation among different slip systems, the graph representing the dislocation network is r-partite, which allows us to consistently orient the graph and relate its orientation to the sign of the junction point density. This ultimately helps in developing the transport equations for open dislocation lines and the junction points for a mean-field description. In these transport equations, the mean-field velocity is assumed to be a prescribed field that is to be determined from the kinetics of the dislocation system. We end with a section on deriving source terms

for the junction point density transport equation.

2. A brief overview of currents

The concept of de Rham currents generalizes Dirac delta distributions, which are localized at a point, to singular objects localized on extended objects, like, e.g., curves or surfaces. Relatively recently, currents have been used in the mathematical modeling of dislocations. Cermelli (1999) showed that, due to their additive group structure, de Rham currents can be used to represent crystal dislocations. In Hochrainer et al. (2007), this additive structure has been employed in ensemble averaging to derive continuum measures of dislocations. In (Epstein and Segev, 2014), a continuum mechanics framework of defects was proposed through the use of currents in which dislocations represent a special case. Olami and Kupferman (2018) used spatial averaging to show that the smooth continuum measure of dislocations is a limit of singular de Rham currents. An important relation regarding dislocation reactions is Frank's second rule at each junction node. Epstein and Segev (2013) used currents to show Frank's second rule can be viewed as a consequence of a topological property, $\partial\partial = \emptyset$, where ∂ denotes the boundary operator on manifolds. They also introduce the idea of a signed point current defined by the boundary of a dislocation line. In the present work we employ currents for averaging and make use of the innate geometrical calculus defined on them, including their connection to conservation laws in terms of Lie derivatives.

Some mathematical preliminaries regarding de Rham currents are introduced first to motivate further developments. A broader introduction to the relevant concepts can be found in (de Rham, 1984) and (Federer and Fleming, 1960). Since we will only be using integral currents, the algebra and calculus of differential forms will be useful and we refer the reader to many texts introducing differential forms (Madsen and Tornehave, 1997; Bott and Tu, 1982; O'Neill, 2006). In the following, all manifolds and submanifolds are always implicitly understood as *oriented* manifolds. We assume an underlying n-dimensional manifold $\mathcal{M}$. Currents on $\mathcal{M}$ are continuous linear functionals on the space of smooth differential forms with compact support in $\mathcal{M}$. Differential forms of degree k may be integrated over k-dimensional sub-manifolds. Given a k-submanifold, $\mathcal{N}$, it defines a k-current, denoted by $T_{\mathcal{N}}$, acting on k-forms θ through

$$T_{\mathcal{N}}[\theta] = \int_{\mathcal{N}} \theta. \tag{1}$$

For obvious reasons, a k-current is said to have dimension k. We will use currents defined this way to represent the singular defects. As discussed in Section 3, averages over such singular objects are expected to yield smooth differential $(n-k)$-forms. The latter constitute the other basic example of k-currents, defined by an $(n-k)$-form ω through,

$$T_{\omega}[\theta] = \int_{\mathcal{M}} \omega \wedge \theta. \tag{2}$$

Dual to the dimension k we call $(n-k)$ the degree of a current. As currents are dual to differential forms, key operations on differential forms induce corresponding operations on currents. We start with the definition of the wedge product

of a current T with a differential form ω, denoted by $T \wedge \omega[\theta]$, and defined by

$$T \wedge \omega[\theta] = T[\omega \wedge \theta]. \tag{3}$$

The reverse order is defined by the antisymmetry property of the wedge product on differential forms, i.e., $\omega \wedge T = (-1)^{pq} T \wedge \omega$ if ω and T are of degree p and q, respectively. The wedge product of two currents is in general not defined. However, for two currents $T_{\mathcal{N}_1}$ and $T_{\mathcal{N}_2}$ originating from two submanifolds $\mathcal{N}_1$ and $\mathcal{N}_2$ of complementary dimension in $\mathcal{M}$, i.e., $\dim(\mathcal{N}_1) + \dim(\mathcal{N}_1) = n$, which only intersect transversally and neither meets the boundary of the other, the wedge product is a 0-dimensional current, which when applied to the constant function 1 yields the oriented intersection number $I(\mathcal{N}_1, \mathcal{N}_2)$ of the (oriented) submanifolds (Guillemin and Haine, 2018),

$$T_{\mathcal{N}_1} \wedge T_{\mathcal{N}_2}[1] = I(\mathcal{N}_1, \mathcal{N}_2). \tag{4}$$

The interior product of a p-current T with vector field $\boldsymbol{X}$ is a $p+1$-current defined by

$$\mathrm{i}_{\boldsymbol{X}} T[\theta] = (-1)^{p+1} T\left[\mathrm{i}_{\boldsymbol{X}} \theta\right]. \tag{5}$$

In the case where the current is defined from a submanifold, the interior product yields a current which can be thought of representing the infinitesimal increment of the submanifold being swept along with the vector field $\boldsymbol{X}$ (Hochrainer et al., 2007).

Stokes theorem for differential forms,

$$\int_{\partial \mathcal{N}} \theta = \int_{\mathcal{N}} d\theta, \tag{6}$$

is used to define both the boundary operator and the exterior differential of currents. The boundary operator on currents is defined as

$$\partial T[\theta] = T[\mathrm{d}\theta], \tag{7}$$

while the exterior derivative on currents is defined as,

$$\mathrm{d}T[\theta] = (-1)^{p+1} T[\mathrm{d}\theta], \tag{8}$$

where the sign may be rationalized from the product rule of the exterior differential. For two currents T_1 and T_2, the dimensions of which add up to $n+1$, one of which has compact support, and if either $\partial T_1 \wedge T_2[1]$ or $T_1 \wedge \mathrm{d}T_2[1]$ is defined, then so is the other and they are equivalent (de Rham, 1984),

$$\partial T_1 \wedge T_2[1] = T_1 \wedge \mathrm{d}T_2[1]. \tag{9}$$

If one of the currents is derived from a differential form and the other from a submanifold this recovers Stokes' theorem; if both currents derive from submanifolds, this yields a generalization of the linking number of curves.

The Lie derivative of a current T is defined through Cartan's formula

$$\mathcal{L}_{\boldsymbol{X}} T = (\mathrm{d}\,\mathrm{i}_{\boldsymbol{X}} + \mathrm{i}_{\boldsymbol{X}}\mathrm{d})\, T. \tag{10}$$

The Lie-derivative occurs in the time evolution of a current induced by a time-dependent (moving) submanifold $\mathcal{N}_t$, whose point-wise motion at $t = 0$ is given by a vector field $\boldsymbol{X}$ defined on $\mathcal{N}_t$. In this case (Hochrainer, 2007; Epstein and Segev, 2014),

$$\left.\frac{d}{dt}\right|_{t=0} T_{\mathcal{N}_t} = -\mathcal{L}_{\boldsymbol{X}} T_{\mathcal{N}}, \tag{11}$$

where the negative sign comes from the product rule of the Lie derivative which yields $\mathcal{L}_{\boldsymbol{X}} T[\theta] = -T[\mathcal{L}_{\boldsymbol{X}}\theta]$.

3. Dislocation systems with reactions

We define junction nodes as points where two or more planar dislocation lines meet. To make clear the relevant definitions, the reader is reminded that dislocation lines are piecewise planar curves on a discrete set of slip planes. A planar closed dislocation line, denoted here by c_{c}, falls completely on a single plane and is not involved in junctions. A planar open dislocation line, denoted here by c_{o}, is one that is not closed on its glide plane and as such meets at common junction nodes with other open lines of the same Burgers vector, as in cross slip, or different Burgers vector, as in junction reactions. Both closed and open dislocation lines are boundaries of planar slipped areas that themselves demarcate the surfaces over which both sides of the crystal have slipped relative to one another by a vector amount equal to Burgers vector. We distinguish the surfaces whose boundaries contain open dislocation lines by calling them open surfaces, denoted by S_{o}, and those whose boundaries a closed dislocation lines by S_{c}. The open surface boundary contains open dislocation lines along with virtual dislocation segments, denoted by c_{v}. The virtual segments denote the lines of intersection of the open slipped surfaces on different slip systems involved in the reaction. We note that we have a virtual dislocation segment for each one of the open surfaces, which covers as a limiting case also when one of the involved open surfaces collapses to the junction line, such that the location of the according open and virtual segment coincide but they have opposite orientation. When the junction segment expands it leaves behind the virtual junction segment which has the opposite orientation to the original junction segment, such that the net Burgers vector of all involved virtual segments along the intersecting line of the involved slip systems always vanishes. These concepts are sketched in Fig. 1. The virtual dislocations naturally appear as part of the boundary of the swept surfaces within the slip planes, but because the net Burgers vector always sums to zero they are in-fact physically non-existent.

The distinctions between closed, open and virtual segments is also reflected in the definition of the dislocation density tensor, $\boldsymbol{\alpha}$. Also this is considered to be made up of slip system contents, $\boldsymbol{\alpha} = \sum_l \boldsymbol{\alpha}^{(l)}_{\mathrm{tot}}$, where the total slip system contribution $\boldsymbol{\alpha}^{(l)}_{\mathrm{tot}}$ contains open, closed, and virtual dislocation line segments. The total dislocation density on a slip system thus corresponds to the boundaries of the slipped areas, as depicted in Figure 1. We further split the slip system dislocation line content into physical and virtual dislocation contributions, $\boldsymbol{\alpha}^{(l)}_{\mathrm{tot}} = \boldsymbol{\alpha}^{(l)} + \boldsymbol{\alpha}^{(l)}_{\mathrm{v}}$, with the physical dislocations including the open and closed lines introduced above. Because the virtual lines cancel upon summation over all slip systems, the total dislocation density is likewise obtained as the sum of only the physical contributions, i.e. $\boldsymbol{\alpha} = \sum_l \boldsymbol{\alpha}^{(l)}$.

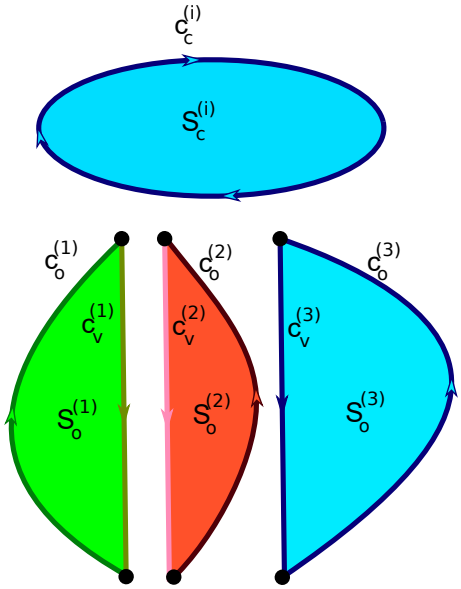

Figure 1: Graphical depiction of the terminology used to distinguish the open and closed line segments, the virtual segments, and the open and closed slipped surfaces.

The physical slip system's dislocation density tensor is defined as a vector valued current through

$$\boldsymbol{\alpha}^{(l)} = \boldsymbol{b}^{(l)} \otimes \left\langle \sum_k T_{c^{(l)}_{c(k)}} + \sum_n T_{c^{(l)}_{o(n)}} \right\rangle \tag{12}$$

where the sum over k is over the closed disjoint dislocation lines embedded in the crystal manifold M (in the sense of Lee (2013)) and the sum over n is over open dislocation lines embedded in M. A similar current denoted by $\boldsymbol{\alpha}_{\mathrm{v}}^{(l)}$ can be constructed for the virtual dislocations, except, in this case, there is only a sum over open line segments. We note again that no dislocation actually ends inside the crystal and that any endpoint of an open segment on a given slip system must be matched by the endpoint of another open segment on a different slip system. Furthermore, we remark that there is an ambiguity in defining the dislocation density current in (12), because reversing the line sense and the Burgers vector simultaneously yields the same vector valued current. This non-uniqueness is eliminated by fixing Burgers vectors *a priori*. In (12), the notation $\langle\cdot\rangle$ refers to the ensemble average. An ensemble is a set of statistically independent and identically distributed random variables and the ensemble averaging yields expectation values of functions of these random variables. Ensemble averaging of currents was first applied to dislocations by Hochrainer et al. (2007); see also Capasso (2018). The average current on the right hand side of (12), defined as

$$\boldsymbol{\rho}^{(l)} = \left\langle \sum_k T_{c^{(l)}_{c(k)}} + \sum_n T_{c^{(l)}_{o(n)}} \right\rangle, \tag{13}$$

is assumed to be generated by a smooth differential 2-form $\boldsymbol{\rho}_{\mathrm{s}}^{(l)}$ such that

$$T_{\boldsymbol{\rho}_{\mathrm{s}}^{(l)}}[\theta] = \boldsymbol{\rho}^{(l)}[\theta]. \tag{14}$$

We remark here that the subscript s refers to the smooth differential form representation of the dislocations. This

convention will be repeated for all other averaged quantities. In a similar fashion a 2-form representing the virtual segments can be constructed and will be denoted by $\boldsymbol{\rho}^{(l)}_{\mathrm{s,v}}$. The dislocation density tensor of the lth slip system now has the form

$$\boldsymbol{\alpha}^{(l)}_{\mathrm{s}} = \boldsymbol{b}^{(l)} \otimes \boldsymbol{\rho}^{(l)}_{\mathrm{s}}. \tag{15}$$

Moreover, as usual in standard coordinates with standard volume element dV, we shall also identify the differential 2-form $\boldsymbol{\rho}^{(l)}_{\mathrm{s}}$ with its generating vector field for which $\boldsymbol{\rho}^{(l)}_{\mathrm{s}} = \mathrm{i}_{\boldsymbol{\rho}^{(l)}_{\mathrm{s}}} dV$ (we make no notational distinction between the 2-form $\boldsymbol{\rho}^{(l)}_{\mathrm{s}}$ and the vector field $\boldsymbol{\rho}^{(l)}_{\mathrm{s}}$). Note that the coefficients of this vector field may be obtained from averaging as

$$\boldsymbol{\rho}^{(l)}_{\mathrm{s}}(\boldsymbol{x}) = \lim_{r\to 0} \frac{1}{\mathrm{Vol}\left(B(\boldsymbol{x},r)\right)} \left\langle \sum_k \boldsymbol{\Delta c}^{(l)}_{\mathrm{c}(k)}\left(B(\boldsymbol{x},r)\right) + \sum_n \boldsymbol{\Delta c}^{(l)}_{\mathrm{o}(n)}\left(B(\boldsymbol{x},r)\right) \right\rangle, \tag{16}$$

where $\boldsymbol{\Delta c}^{(l)}_{\mathrm{c}(k)}\left(B(\boldsymbol{x},r)\right)$ denotes the connecting vector from the point of entry of a dislocation into the ball $B(\boldsymbol{x},r)$ centered at $\boldsymbol{x}$ with radius r to where it leaves the ball. Such a vector is identically zero if the segment does not intersect the ball. In the sum over open dislocation lines, $\boldsymbol{\Delta c}^{(l)}_{\mathrm{o}(n)}\left(B(\boldsymbol{x},r)\right)$ connects the points of entry and leaving or, if the segment starts or ends in the ball, it connects the intersection point with the surface of the ball and the boundary point inside the ball, directed in accordance with the line-sense of the curve. We refer the reader to Hochrainer et al. (2007) for more details on the definition of smooth objects from averages over currents. See also Weger et al. (2021) for practical applications of these concepts to discrete dislocation data.

We now define the plastic distortion current by its slip system constituents $\boldsymbol{\beta}^p = \sum_l \boldsymbol{\beta}^{p(l)}$. Each slip system current contribution is defined by

$$\boldsymbol{\beta}^{p(l)} \equiv \boldsymbol{b}^{(l)} \otimes \left\langle \sum_k T_{S^{(l)}_{\mathrm{c}(k)}} + \sum_n T_{S^{(l)}_{\mathrm{o}(n)}} \right\rangle, \tag{17}$$

where the sum over k and n, respectively, signify the sum over all closed and open slipped surfaces embedded in M. The current on the right hand side of (17), which given by

$$\boldsymbol{\gamma}^{(l)} = \left\langle \sum_k T_{S^{(l)}_{\mathrm{c}(k)}} + \sum_n T_{S^{(l)}_{\mathrm{o}(n)}} \right\rangle, \tag{18}$$

is assumed to yield a smooth differential 1-form defined such that

$$T_{\boldsymbol{\gamma}^{(l)}_{\mathrm{s}}}[\theta] \equiv \boldsymbol{\gamma}^{(l)}[\theta]. \tag{19}$$

In the last expression, $T_{\boldsymbol{\gamma}^{(l)}_{\mathrm{s}}}$ is the current defined by the differential 1-form, $\boldsymbol{\gamma}^{(l)}_{\mathrm{s}}$. This 1-form can be identified with a vector field via the standard metric. Using virtual dislocation segments and the definitions of the dislocation density tensor and the plastic distortion, which now contain open and closed segments, we can reach the classic integral relationship $\int_F \boldsymbol{\alpha} = \int_{\partial F} \boldsymbol{\beta}^p$. To show this, we first observe the following geometric relations for a given open surface S_{o}, see Fig. 1:

$$\begin{aligned} c_{\mathrm{o}} &= \partial S_{\mathrm{o}} - c_{\mathrm{v}} \\ \partial c_{\mathrm{o}} &= -\partial c_{\mathrm{v}}. \end{aligned} \tag{20}$$

This allows us to rewrite (12) as

$$\boldsymbol{\alpha}^{(l)} = \boldsymbol{b}^{(l)} \otimes \left\langle \sum_k T_{\partial S^{(l)}_{\mathrm{c}(k)}} + \sum_n T_{\partial S^{(l)}_{\mathrm{o}(n)}} - \sum_n T_{c^{(l)}_{\mathrm{v}(n)}} \right\rangle \tag{21}$$

$$= \boldsymbol{b}^{(l)} \otimes \partial \left\langle \sum_k T_{S^{(l)}_{\mathrm{c}(k)}} + \sum_n T_{S^{(l)}_{\mathrm{o}(n)}} \right\rangle - \boldsymbol{b}^{(l)} \otimes \left\langle \sum_n T_{c^{(l)}_{\mathrm{v}(n)}} \right\rangle =: \boldsymbol{\alpha}^{(l)}_{\mathrm{tot}} - \boldsymbol{\alpha}^{(l)}_{\mathrm{v}}, \tag{22}$$

where we have used (20) and the fact that the boundary operator is a continuous linear map of currents, see (de Rham, 1984), which commutes with the ensemble averaging operation. Since the virtual segments collectively vanish upon summation over the slip systems, the total dislocation density tensor takes on the form

$$\boldsymbol{\alpha} = \sum_l \boldsymbol{\alpha}^{(l)} = \sum_l \left[\boldsymbol{b}^{(l)} \otimes \partial \left\langle \sum_k T_{S^{(l)}_{\mathrm{c}(k)}} + \sum_n T_{S^{(l)}_{\mathrm{o}(n)}} \right\rangle \right]. \tag{23}$$

We can have the vector current $\boldsymbol{\alpha}$ act on a current T_F which represents the area element that bounds the Burgers circuit, denoted by $\boldsymbol{\alpha} \wedge T_F[1]$. Using property (9) and $\mathrm{d}T_F = (-1)^2 \partial T_F = T_{\partial F}$, we may write

$$\boldsymbol{\alpha} \wedge T_F[1] = \sum_l \left[\boldsymbol{b}^{(l)} \otimes \partial \left\langle \sum_k T_{S^{(l)}_{\mathrm{c}(k)}} + \sum_n T_{S^{(l)}_{\mathrm{o}(n)}} \right\rangle \wedge T_F[1] \right] \tag{24}$$

$$= \sum_l \left[\boldsymbol{b}^{(l)} \otimes \left\langle \sum_k T_{S^{(l)}_{\mathrm{c}(k)}} + \sum_n T_{S^{(l)}_{\mathrm{o}(n)}} \right\rangle \wedge T_{\partial F}[1] \right] \tag{25}$$

$$= \sum_l \left[\boldsymbol{\beta}^{p(l)} \right] \wedge T_{\partial F}[1] \tag{26}$$

$$= \boldsymbol{\beta}^p \wedge T_{\partial F}[1], \tag{27}$$

which is equivalent to $\int_F \boldsymbol{\alpha}_{\mathrm{s}} = \int_{\partial F} \boldsymbol{\beta}^p_{\mathrm{s}}$. We may interpret this expression in terms of currents as the equality of the signed intersections of dislocations with the Burgers surface to the signed intersections of the circuit with the slipped surface. This is illustrated in Fig. 2. We note that this method of measuring signed intersections via the integral relation $\int_F \boldsymbol{\alpha}_{\mathrm{s}} = \int_{\partial F} \boldsymbol{\beta}^p_{\mathrm{s}}$ can equally be used as a definition of the dislocation density tensor. This is, in fact, how the dislocation density tensor is defined in the classical literature, which reads in differential form notation

$$\boldsymbol{\alpha}_{\mathrm{s}} = \mathrm{d}\boldsymbol{\beta}^p_{\mathrm{s}}\,. \tag{28}$$

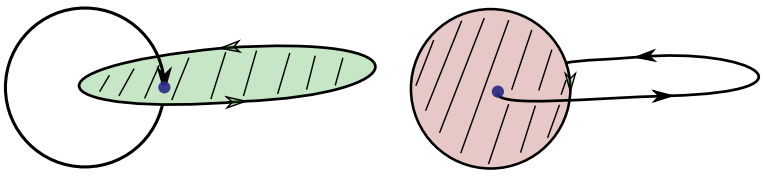

Figure 2: Depiction of the signed intersection of a dislocation line with the Burgers surface (in green) and the signed intersection of the Burgers circuit with the slipped area (in red).

Note that when considering junctions, this relation holds for the total dislocation density, while on the slip system level, the exterior derivative of the accumulated plastic slip contains the virtual segments, i.e. we have

$$\boldsymbol{\alpha}^{(l)}_{\mathrm{s}} + \boldsymbol{\alpha}^{(l)}_{\mathrm{s,v}} = \mathrm{d}\boldsymbol{\beta}^{p(l)}_{\mathrm{s}} \tag{29}$$

because each slip system may contain dislocations that are open. Taking the exterior derivative of the last expression and noting that the Burgers vector is constant we arrive at a constraint on each slip system of the form

$$\mathrm{d}\boldsymbol{\rho}_{\mathrm{s}}^{(l)} + \mathrm{d}\boldsymbol{\rho}_{\mathrm{s,v}}^{(l)} = 0. \tag{30}$$

This constraint reflects that the 2-form $\boldsymbol{\rho}_{\mathrm{s}}^{(l)}$ represents open and closed lines. In the case where there are only closed dislocation lines, this expression reduces to $\mathrm{d}\boldsymbol{\rho}_{\mathrm{s}}^{(l)} = 0$. The constraint (30) will become important when numerically solving the transport equations for $\boldsymbol{\rho}_{\mathrm{s}}^{(l)}$. While the virtual density naturally occurs when connecting to the plastic slip per slip system, we will see in the next section that the virtual dislocations and their density may be replaced by the proper state variables of endpoints and endpoint densities when modeling the evolution of the dislocation system.

4. Measure of dislocation reactions

When dislocations react and form complex networks, the set consisting of the dislocation lines is in general not a one-dimensional manifold. This fact can be seen by analyzing the location of the triple junction point in Fig 3. It has three arms extending from it, and thus an open neighborhood around this point is not one dimensional, and therefore not homeomorphic to R^1 at the junction point. It does, however, decompose into zero and one dimensional manifold parts (dislocation lines being one dimensional if we split each line at the junction point). Likewise, the slipped areas can be decomposed by splitting along the virtual dislocation segments. All the theorems involving manifolds and submanifolds, like (11), can be applied to the manifold parts of the dislocation system but there should be a relationship tying together the manifold parts, e.g. junction arms to junction points.

The kinematic evolution of junctions involves the reaction of two dislocations over a finite segment with two junction nodes as well as the motion of these nodes. Fig. 3 illustrates this process, which is elaborated mathematically later.

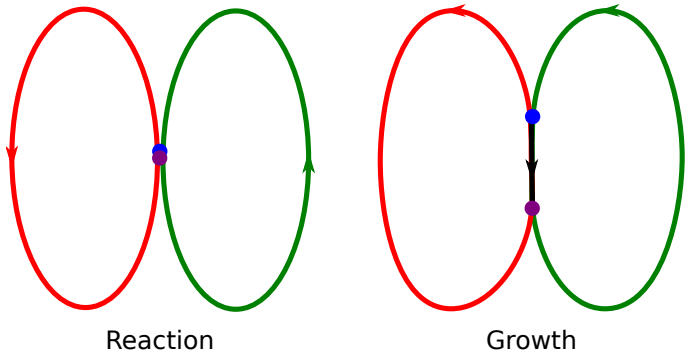

Figure 3: Depiction of the junction formation process, which starts with the creation of two overlapping junction nodes and then the progressive growth of the junction segment by the separation of the junction nodes.

An important relation between junction arms and junction points is Frank's second rule (Hirth et al., 1983), which states that the sum of Burgers vectors entering into a junction node must be equal to the sum of Burgers vectors exiting

the node. Frank's second rule is important in describing junctions and other network-forming processes in general. At a single junction node P, this rule is written in terms of currents as a sum over the connecting (open) dislocation arms $c_{\mathrm{o}}^{(i)}$, i.e. with positive or negative end-point at P, as

$$\sum_{i:\,\pm P\in\partial c_{\mathrm{o}}^{(i)}} T_{\partial c_{\mathrm{o}}^{(i)}}(P)\boldsymbol{b}^{(i)} := \sum_{i:\,\pm P\in\partial c_{\mathrm{o}}^{(i)}} \mathrm{sgn}_P(\partial c_{\mathrm{o}}^{(i)})\boldsymbol{b}^{(i)} = 0\,, \tag{31}$$

where, by abuse of notation, we use the point P as argument of the currents on the left hand side. This notation is interpreted as determining the signs of the oriented boundary points located at the junction point P, as denoted by the function $\mathrm{sgn}_P(\partial c_{\mathrm{o}}^{(i)})$ on the right hand side.

This section describes how the endpoint densities of dislocations on all slip systems are described. The current representation of the endpoints is the vector valued 0-current, which is defined by

$$\boldsymbol{\Pi}^{(l)} \equiv -\boldsymbol{b}^{(l)} \otimes \left\langle \sum_n T_{\partial c_{\mathrm{o}(n)}^{(l)}} \right\rangle. \tag{32}$$

Since $\partial c_{\mathrm{c}} = \emptyset$, the latter can be written as

$$\boldsymbol{\Pi}^{(l)} = -\boldsymbol{b}^{(l)} \otimes \partial \left\langle \sum_k T_{c_{\mathrm{c}(k)}^{(l)}} + \sum_n T_{c_{\mathrm{o}(n)}^{(l)}} \right\rangle. \tag{33}$$

Ensemble averaging then yields a smooth differential form $\pi_{\mathrm{s}}^{(l)}$ of degree 3 such that

$$\pi^{(l)} = -\partial \left\langle \sum_k T_{c_{\mathrm{c}(k)}^{(l)}} + \sum_n T_{c_{\mathrm{o}(n)}^{(l)}} \right\rangle, \tag{34}$$

and

$$\pi^{(l)}[\theta] \equiv T_{\pi_{\mathrm{s}}^{(l)}}[\theta] = \int_M \pi_{\mathrm{s}}^{(l)} \wedge \theta. \tag{35}$$

Following Hochrainer et al. (2007), the smooth form, $\pi_{\mathrm{s}}^{(l)}$, can be obtained from averages over currents which allows us to interpret the smooth form as the signed sum of endpoints of dislocation lines on slip system l at a given point in space. This interpretation may also be inferred from (32). Comparing (12) and (33), it is easy to see that $T_{\boldsymbol{\Pi}_{\mathrm{s}}^{(l)}} = \partial T_{\boldsymbol{\alpha}_{\mathrm{s}}^{(l)}} = T_{\mathrm{d}\boldsymbol{\alpha}_{\mathrm{s}}^{(l)}}$. We note here that

$$\boldsymbol{\Pi}_{\mathrm{s}}^{(l)} = \mathrm{d}\boldsymbol{\alpha}_{\mathrm{s}}^{(l)} \tag{36}$$

because we have defined the endpoints in (32) to be oriented opposite of the orientation given by the boundary operator.

The relationship (36) can also be shown using the product property (9) to produce $\int_{\partial V} \boldsymbol{\alpha}_{\mathrm{s}}^{(l)} = \int_V \boldsymbol{\Pi}_{\mathrm{s}}^{(l)}$. This can be shown by writing the intersection product as $\boldsymbol{\alpha}^{(l)} \wedge T_{\partial V}[1] = \boldsymbol{\Pi}^{(l)} \wedge T_V[1]$. The above relationship is thus interpreted as the differential form equivalent to the equality of the signed intersections of open lines with the closed surface ∂V to the signed intersection of endpoints within the volume V. This is shown in Fig. 4. Given the intersection relationship we can alternatively define the endpoint densities based upon (36). This definition will aid our understanding when we look at these measures at different lengths scales in Section 5. As we can write $\Pi_{\mathrm{s}}^{(l)}$ in the form

$$\boldsymbol{\Pi}_{\mathrm{s}}^{(l)} = \boldsymbol{b}^{(l)} \otimes \pi_{\mathrm{s}}^{(l)}, \tag{37}$$

it follows from (35) that

$$\pi_{\mathrm{s}}^{(l)} = \mathrm{d}\boldsymbol{\rho}_{\mathrm{s}}^{(l)}. \tag{38}$$

The constraint (30) can then be written as $\pi_{\mathrm{s}}^{(l)} = \mathrm{d}\boldsymbol{\rho}_{\mathrm{s}}^{(l)} = -\mathrm{d}\boldsymbol{\rho}_{\mathrm{s,v}}^{(l)}$ and thus introducing the endpoint removes the need to model the virtual dislocation segments. In a vector field notation, (38) may be written as $\pi_{\mathrm{s}}^{(l)} = \mathrm{div}\boldsymbol{\rho}_{\mathrm{s}}^{(l)}$. From the closedness of the total dislocation density tensor we have

$$\mathrm{d}\boldsymbol{\alpha}_{\mathrm{s}} = \sum_l \boldsymbol{\Pi}_{\mathrm{s}}^{(l)} = 0, \tag{39}$$

which we rewrite as

$$\sum_l \mathrm{d}\boldsymbol{\rho}_{\mathrm{s}}^{(l)} \boldsymbol{b}^{(l)} = \sum_l \pi_{\mathrm{s}}^{(l)} \boldsymbol{b}^l = 0. \tag{40}$$

We interpret this as the continuum counterpart to Frank's second rule, saying that sums of Burgers vectors at all junctions cancel.

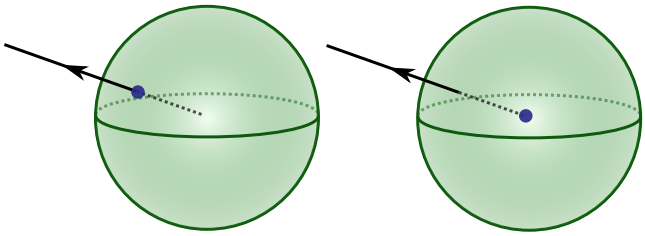

Figure 4: Depiction of the signed intersection of the open dislocation line with the closed surface (boundary of the sphere) and the signed intersection of the endpoint with the volume of the sphere.

So far, we have introduced density measures to describe endpoints of open dislocation lines on various slip systems of a crystal. We note here that the endpoints of open lines on different slip systems are coupled since they relate to the junction points, which is reflected in (40). We also note that every endpoint may be assigned to a junction point and that we may accordingly introduce currents and differential forms for the junction points. It is further important to realize that the endpoints inherit an orientation or sign (used interchangeably in the sequel) from the orientation of the dislocation line and that the junction points are signed objects, where the sign needs to be determined from the signs of the contributing endpoints. For this reason, we need to develop a way to orient the junction nodes and to ensure consistency of such an orientation. We delay discussing the issue of a consistent orientation until the next section where we introduce graphs to represent the dislocation networks.

Let us denote junction points locations as $P_{(j)}^{(pqr)}$, where j is an index labeling the points. We exclusively work with three-armed junctions and label the Burgers vectors of the involved arms by p, q, and r. As will be discussed in Section 6, a meaningful definition of the junction point sign is given by the product of the signs of the connecting arms, i.e.,

$$\mathrm{sgn}(P_{(j)}^{(pqr)}) \coloneqq \mathrm{sgn}_P(\partial c_{\mathrm{o}(j)}^{(p)})\mathrm{sgn}_P(\partial c_{\mathrm{o}(j)}^{(q)})\mathrm{sgn}_P(\partial c_{\mathrm{o}(j)}^{(r)}), \tag{41}$$

where $\mathrm{sgn}_P(\partial c^{(p)}_{\mathrm{o}(j)})$ denotes the sign of the endpoint of the dislocation line $c^{(p)}_{\mathrm{o}(j)}$ involved in the jth junction point. Given the sign $\mathrm{sgn}(P^{(pqr)}_{(j)})$ of the junction point j, the junction point current is defined as

$$\pi^{pqr}_{\mathrm{J}} = \left\langle \sum_j \mathrm{sgn}(P^{(pqr)}_{(j)}) T_{P^{(pqr)}_{(j)}} \right\rangle. \tag{42}$$

We note that in the above expression, $T_{P^{(pqr)}_{(j)}}$ is an unsigned, i.e., positive current. We can make use of the ensemble average again to obtain a smooth 3-form representing this current. This form contains the signed sum of junction points at a given point in space. An example for the junction point orientation is shown in the Fig. 5. We note the importance of the sign being dependent on whether the lines point into or out of the junction point. Consequently, when the network evolves in time, the sign of the junction point does not change. We will see that the definition of the junction point sign given by (41) is consistent with a coloring property of the graphs created by dislocations when we are only considering one junction group involving a triplet of Burgers vectors as is the case in face-centered cubic (FCC) crystals. We will thus be able to form a correspondence between the endpoints and signed junction points. When multiple types of junctions are considered more care is needed to establish a relationship between the endpoints and junction points. This is touched upon in Section 7.

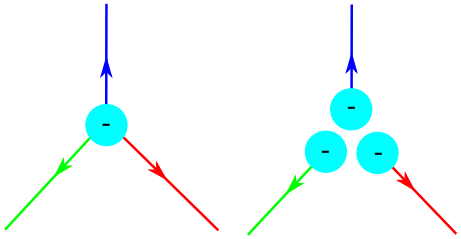

Figure 5: Depiction of the particular case where the orientation of the junction node (on the left) is the same as the orientations of the endpoint densities (on the right). The orientation is denoted by the blue color of the dot which represents the location of the junction node (on the left) and 3 endpoint nodes (on the right).

5. Length scale considerations

The signed nature of endpoints and junction point densities stems from the fact that they are defined from oriented intersections, see (28) and (35). The corresponding densities are thus geometric quantities that depend on the length scale over which they are defined. In a dense dislocation systems, these densities measure the net number of end points and junction points. The sign issue arises also in the representation of the endpoint and junction point currents, as in (13), (18), and (42) where the averaged currents are defined by summing over oriented submanifolds. Following the terminology in dislocation theory we refer to the net densities as geometrically necessary.

Due to the signed nature, defining these net densities is always tied to length scale resolution much like in defining the dislocation density tensor, $\boldsymbol{\alpha}$. Hence, a problem that might arise when considering a model that contains the endpoint and junction point densities, along with the dislocation densities, is the difference in the length scale at which each of these density measures can accurately represent the dislocation network. When referring to a length scale, it

is convenient to view the intersection product definitions of the density measures like in (36) and (28). When using intersections to define the density measures, the length scale of the model is a characteristic length associated with the submanifold used to measure intersections. For instance, in the intersection definition of the endpoint densities (36), the characteristic length would be the radius of the solid sphere used to intersect with the endpoints. Another example is the radius of the Burgers circuit used in the definition of the dislocation density tensor in (28). The question now is whether or not a length scale used to define the geometrically necessary dislocation densities (GND) overlaps with those associated with the geometrically necessary endpoint or geometrically necessary junction point densities. For simplicity, we will call the latter the endpoint and junction point densities.

We begin the consideration of the length scale issue posed above with motivating the use of the junction point densities rather than the endpoint densities, using a specific example. The signed nature of endpoints make their geometric density dependent upon the length scale resolution of the model. This is depicted in Fig. 6, where we describe two scenarios which have in common one dislocation type (the red line) which enters both junction points with opposite orientations. In both parts of the figure, this would look like a closed line on larger length scale for the slip system that shares the common arm; thus after integrating over the surface of the solid sphere, V, we have $\int_{\partial V} \boldsymbol{\rho}_{\mathrm{s}}^{(3)} = 1-1 = 0$ where we have used the intersection of the open dislocation lines with ∂V to evaluate this integral. If we were using the endpoints to model the dislocation system then the information about the multiple types of junctions would be lost from the perspective of this slip system due to the fact that $\int_V \mathrm{d}\boldsymbol{\rho}_{\mathrm{s}}^{(3)} = 0$. Now consider the right part of Fig. 6. If we represent the system using junction point densities we obtain $\int_V \mathrm{d}\boldsymbol{\rho}_{\mathrm{s}}^{(3)} = \int_V \pi_{\mathrm{sJ}}^{(123)} + \pi_{\mathrm{sJ}}^{(345)} = 1 - 1 = 0$ where we have used intersections to evaluate both integrals. That is, we still have $\int_V \mathrm{d}\boldsymbol{\rho}_{\mathrm{s}}^{(3)} = 0$ but we retain the information about the junction points. This problem arises because $\boldsymbol{\rho}_{\mathrm{s}}^{(3)}$ is involved in more than one junction type. Therefore, the specification of the endpoint density does not lead to a unique specification of junction point densities. This issue can be solved by modeling the state of the system with the junction point densities instead of the endpoint densities and this is the approach taken in this paper. In the specific example given in the right part of Fig. 6 we noted that $\int_V \mathrm{d}\boldsymbol{\rho}_{\mathrm{s}}^{(3)} = \int_V \pi_{\mathrm{sJ}}^{(123)} + \pi_{\mathrm{sJ}}^{(345)}$ which implies that $\pi_{\mathrm{s}}^{(3)} = \pi_{\mathrm{sJ}}^{(123)} + \pi_{\mathrm{sJ}}^{(345)}$. In subsequent sections we will show why we expect such a relation to exist and give a more general expression between the endpoints and junction points.

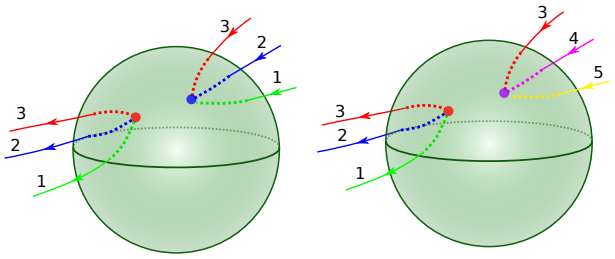

Figure 6: Illustration of the loss of information that end point density causes when multiple junction types are present. In the left figure, the red, blue and green lines appear continuous due to cancellation of endpoints for each color. In the right part, the red line appears continuous for the same reason but the other colors have net endpoints.

The definition of the junction point density may also suffer from cancellations when defined on the same length

scale as the dislocation density vector. To illustrate this we refer to low energy dislocation structures observed in rolled aluminum (Hong et al., 2013; Winther et al., 2015), where we can observe a potential discrepancy in the length scales over which the dislocation, endpoint and junction point densities are representative of the system at the same time. To illustrate such a discrepancy, we modify a figure from Winther et al. (2015) to produce Fig. 7. In doing so, the inclusion of the junction points as a signed measure is made clear by assigning them the red and blue colors. This will serve our purpose of introducing graphs representing the dislocation networks later. For now, we observe in Fig. 7 that the line orientation of all dislocation segments of every color is along one direction and thus the corresponding dislocation density vectors are representative of this system at the depicted scale (roughly 200nm). However, the junction point densities corresponding to the red and blue colors vary at a shorter length scale and thus the geometric junction point density would not accurately represent the system. From this discussion it can be seen that the net number of junction points in the volume depicted in the figure, which is suited for the vector density description, is not representative of the total number of junction points in the same volume. Due to the signed nature of these junction points, there is a geometric cancellation and statistical storage.

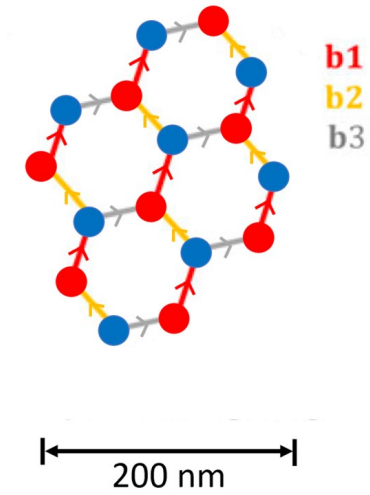

Figure 7: A figure adopted from Winther et al. (2015) depicting a low energy dislocation structure involving dislocations of three Burgers vectors represented by three different colors. The dots are junction points. The scale of the part of the network shown is on the order of 200nm.

In order to have a dislocation network model consistent with the line bundle picture of continuum dislocation dynamics (Anderson and El-Azab, 2021), we shall, therefore, represent the endpoints in terms of positive and negative densities whose difference is the geometric density. This is possible because each of the $T_{\partial c^{(l)}_{o(n)}}$ currents in (32) represent both the positive and negative endpoints of each open dislocation line respectively. Since the endpoints of an open dislocation line are in different locations we can represent using separate points and thus define two new signed currents corresponding to each of these points. We proceed analogously for the junction point density. We thus write

$$\pi_{\mathrm{s}}^{(l)} = \pi_{\mathrm{s}}^{(l)+} - \pi_{\mathrm{s}}^{(l)-}, \quad \pi_{\mathrm{sJ}}^{(pqr)} = \pi_{\mathrm{sJ}}^{(pqr)+} - \pi_{\mathrm{sJ}}^{(pqr)-}. \tag{43}$$

In this representation we retain the information of positive and negative endpoints and junction points, which makes their density representation consistent with the dislocation density from a length scale perspective.

In the next section we establish a unique connection between the signed endpoint densities and the signed junction point densities.

6. Graph theoretic approach to dislocation networks

This section has two objectives, to introduce the dislocation network in terms of graph theory and use the tools of the latter theory to interpret and derive relations for the continuum representation of dislocations. This is important for establishing a relationship between the sign of the junction point density and the sign of the corresponding endpoint densities.

A graph G is a pair $G = (V, E)$ of lists. V is a list of vertices (nodes) and $E \subseteq V \times V$ a list of pairs of vertices called edges. A graph is called r-partite if its vertex set can be split into r disjoint sets $V_1, V_2, .., V_r$ such that every edge connects a pair of vertices from two different sets. This means that vertices in a given set are not adjacent (Diestel, 2017). A graph that can be split into two sets of vertices in this manner is called a bipartite graph. In this case the sets of vertices may be identified by a sign, which is why this property relates to the signed junction points in the current case. The property of a graph being bipartite or not may be checked by counting edges along closed paths in the graph – so called cycles. A path is a sequence of edges joining disjoint sets of vertices, typically denoted by a list of vertices. A cycle is a path which starts and ends at the same vertex and contains any edge at most one time. When considering whether a graph is bipartite we can equivalently show that there are no odd length cycles (Diestel, 2017), where the length of the cycle is the number of edges in the cycle.

Dislocation networks in crystals can be easily represented by graphs. For analysing the properties of graphs which represent dislocation networks we focus here on junction formation in FCC crystals. In such crystals, there are four distinct slip planes, commonly denoted by A,B,C, and D. In each plane there are 3 slip directions identified with Burgers vectors. Due to symmetry considerations, there are only six unique Burgers vector, denoted $b_1, b_2, \ldots, b_6$. We follow Akhondzadeh et al. (2021) in using the Schmid and Boas (SB) notation for slip systems. In this notation, the slip normal and Burgers vector are paired. For example A3 denotes a slip system with slip plane A and Burgers vector b_3. A summary of FCC slip systems (and their glissile reactions, see below) in this notation is given in Table 1. According to Schmid and Boas (1968), junctions are classified into sessile and glissile types. If the resulting dislocation junction is in one of the twelve slip systems given in Table 1 then the junction is glissile. Otherwise, the junction is sessile. The latter junctions are either of Lomar type or of Hirth type (Hirth et al., 1983). A coplanar junction is one in which the Burgers vectors of the dislocation lines ending at the junction point fall in the same plane. When two dislocations on different slip planes have the same Burgers vector they may react to annihilate each other. This reaction is called collinear annihilation.

To fix ideas, we only consider glissile junctions with three-armed junction nodes in this communication. However, as discussed later, the final results are general and apply when all other networking mechanisms are present. We start

Table 1: Slip systems in FCC crystals in Schmid-Boas (SB) notion. The last column denotes the SB index for the reacting systems that produce a glissile junction segment on this row's slip system. The table is modified from (Akhondzadeh et al., 2021).

Index	Slip plane	b	SB index	Glissile reaction
1	$(\bar{1}11)$	$\frac{1}{2}[0\bar{1}1]$	A2	A3+D6,A6+C3
2	$(\bar{1}11)$	$\frac{1}{2}[101]$	A3	A2+D6, A6+B2
3	$(\bar{1}11)$	$\frac{1}{2}[110]$	A6	A2+C3, A3+B2
4	(111)	$\frac{1}{2}[0\bar{1}1]$	B2	B4+C5, B5+D4
5	(111)	$\frac{1}{2}[\bar{1}01]$	B4	A2+B5, B2+C5
6	(111)	$\frac{1}{2}[\bar{1}10]$	B5	A2+B4, B2+D4
7	$(\bar{1}\ \bar{1}1)$	$\frac{1}{2}[011]$	C1	A3+C5, B5+C3
8	$(\bar{1}\ \bar{1}1)$	$\frac{1}{2}[101]$	C3	B5+C1, C5+D1
9	$(\bar{1}\ \bar{1}1)$	$\frac{1}{2}[\bar{1}10]$	C5	A3+C1, C3+D1
10	$(1\bar{1}1)$	$\frac{1}{2}[011]$	D1	A6+D4, B4+D6
11	$(1\bar{1}1)$	$\frac{1}{2}[\bar{1}01]$	D4	A6+D1, C1+D6
12	$(1\bar{1}1)$	$\frac{1}{2}[110]$	D6	B4+D1, C1+D4

by requiring a vertex or a node in the graph representing the dislocation network to correspond to the junction point. The open dislocation lines connecting the junction points are taken to be the edges of the graph. As explained below, the graph created in this fashion is r-partite. Fig. 8 shows some glissile junction reaction among multiple dislocation loops that form a network, which is represented by a graph. Regardless of the Burgers vector types involved, the junction starts at the intersection point of two reacting dislocations then splits into two vertices connected by a new edge. The junction segments are differentiated by their color, which signifies the different Burgers vectors of the lines corresponding to the edges. We note that the list of edges in the graph contain non-unique entries. For example, edges 1 and 2 both share the same vertices, as well as edges 5 and 6. Graphs with this property are called multigraphs (Diestel, 2017).

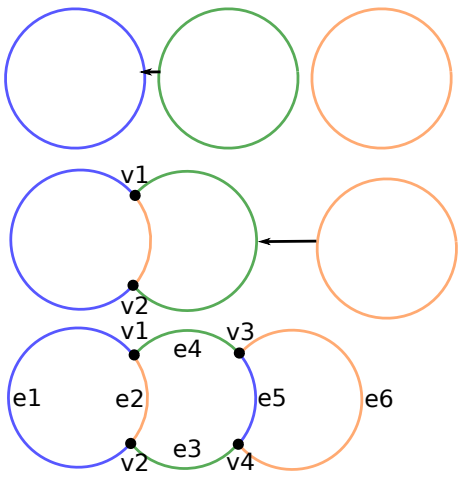

Figure 8: An illustration of coplanar junction formation in FCC crystals using graphs. Three loops (top) are about to react. The green and blue loops react to form the orange dislocation segment connecting the junction nodes (middle). Next, the open green line and the orange loop react to form a blue junction segment (bottom).

Before moving on, we define some terminology that will become important when talking about the graphs representing dislocation networks. We define a dislocation junction group to be a triplet of different Burgers vectors that correspond to a glissile junction reaction. We also define a junction type to be a triplet of different slip systems. With this terminology each junction group contains multiple junction types. For instance, the glissile reactions A2+A3+D6 and A2+C3+A6 both form different junction types but since the Burgers vectors involved in these reactions are the same, they are also in the same junction group. When only considering one junction group, we cannot allow one loop to react with two edges connected to the same junction node. The reasoning for this is given in Appendix A.

The graph created by a given junction group is bipartite. We can prove this by showing that all cycles in the graph are even. To do so we consider two cases, one where the dislocations involved in the reaction are in two different connected components in the graph, like in Fig. 8, and another where they are in the same connected component. Two vertices are considered to be in the same connected component if there is a path connecting them. We start with the case where the edges are in different connected components. We create a cycle by first starting with an arbitrary edge, say e_6, of the final graph in Fig. 8, now isolated in Fig.9. For the cycle to be of even length, the dotted path length from node v_3 to v_4 must be odd because odd + odd = even. For this example, we can evaluate all the remaining paths and show that they are of odd length. For an arbitrary graph, though, we rely on the fact that each additional junction reaction added to the graph gives 2 additional odd-length paths. In Fig. 8 the path from vertex v1 to v2, in the middle part has odd length equal to one (every path from v1 to v2 has to be odd because they are adjacent and thus in different vertex sets). In the lower part of the figure, a junction segment is added between vertices v1 and v2. In doing so, an alternative odd-length paths from v1 to v2 is added. Since the junction reaction preserves the oddness property of paths lengths between the points involved in the reaction, any subsequent junction reaction does not alter the bipartite property of the graph. Since the junction group consists of multiple junction types, the bipartite vertex sets can be further decomposed into different junction types. In the following we focus primarily on the bipartite vertex sets because they will be important for establishing orientation relations between junction points and endpoints.

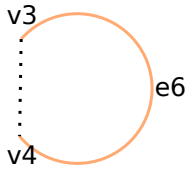

Figure 9: An arbitrary chosen edge of the dislocation network shown in Fig. 8. The dotted lines denote the possible paths that create a cycle with the inclusion of edge e_6.

In the case where the reacting edges are in the same connected component we refer to Fig 10, where the vertex sets are assigned positive and negative signs. Looking at the graph we see that the vertex sets containing v1, v2, v3, and v4 are left unchanged after the reaction because the additional paths from v1 to v2 have odd lengths and the additional paths from v4 to v1 also have odd lengths. We also have additional vertices, v5 and v6, that have been added to the graph which are consistent with the bipartite property of the graph.

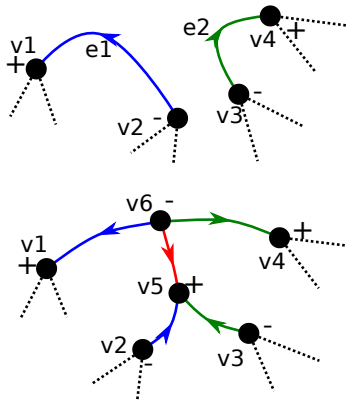

Figure 10: A depiction of junction formation when reacting segments come from the same connected component of the graph. The dotted lines represent connectivity with the rest of the graph not shown in the figure.

An important property of bipartite graphs is that they are 2-colorable (Diestel, 2017). By 2-colorable it is meant that a color can be assigned to each vertex so that pairs of adjacent vertices do not share the same color. The bipartite property also provides us with an easy way to recover the directed graph of the dislocation network by specifying rules for line directions into or out of the vertices. Consider, for example, the 2-colorable graph in Fig.11 where we show an undirected graph in the left part. By specifying that all edges should point towards the green-colored vertices and away from every adjacent red-colored vertices, we recover the directed graph to the right of the figure. For this reason, we use color and orientation interchangeably.

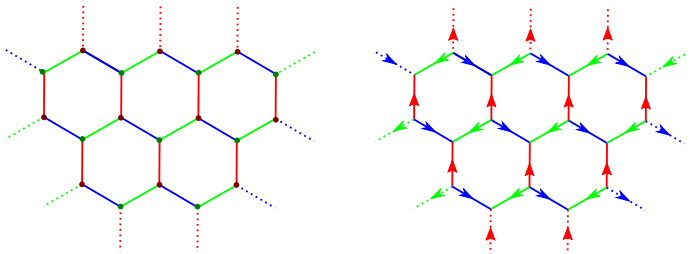

Figure 11: Depiction of the recovery of a directed graph from an undirected graph given a set of rules for how the lines should be directed base on the coloring of the edges. The dashed lines denote connections to the other junction points not shown in the figure.

We are more interested in less arbitrary ways of providing rules for the orientations of edges connecting the vertices in the dislocation network graph. We can provide rules for these orientations using Frank's second rule, given by (31), at each vertex. For instance, the graph in Fig. 11 would also be created when we fix the Burgers vectors such that

$$\boldsymbol{b}^{(1)} + \boldsymbol{b}^{(2)} + \boldsymbol{b}^{(3)} = 0. \tag{44}$$

In Fig.11, we color the edges with Burgers vector $\boldsymbol{b}^{(1)}$ green, those with Burgers vector $\boldsymbol{b}^{(2)}$ blue, and the edges with Burgers vector $\boldsymbol{b}^{(3)}$ red. With the Burgers vectors fixed in this way, there would only be two types of junction nodes (vertices), those with all the segments pointing into the vertices and those with all the segments pointing out. If we

now fix the Burgers vectors such that

$$\boldsymbol{b}^{(1)} + \boldsymbol{b}^{(2)} - \boldsymbol{b}^{(3)} = 0, \tag{45}$$

then one set of vertices would have edges with $\boldsymbol{b}^{(1)}$ and $\boldsymbol{b}^{(2)}$ pointing into while $\boldsymbol{b}^{(3)}$ is pointing out of the vertices, and another set having $\boldsymbol{b}^{(1)}$ and $\boldsymbol{b}^{(2)}$ directed out while $\boldsymbol{b}^{(3)}$ directed into the vertices.

We now recall the definition of the sign of the junction point current in (41). Here we show that such a definition corresponds to the bipartite property of the graph. This can be shown for both of the examples mentioned above. In the first, $\boldsymbol{b}^{(1)} + \boldsymbol{b}^{(2)} + \boldsymbol{b}^{(3)} = 0$ and the sign of the junction point determined from (41) is the same as the sign of each endpoint. In this case, we trivially recover the bipartite property because every adjacent node has a different orientation. In the second example, $\boldsymbol{b}^{(1)} + \boldsymbol{b}^{(2)} - \boldsymbol{b}^{(3)} = 0$. From the 3-term product in (41), we know that 2 of the terms have the same sign. Therefore, the sign of their product does not contribute to the junction point sign; the third term, however, determines that sign. We can then view the set of edges with Burgers vectors given by $\boldsymbol{b}^{(3)}$ as providing the sign of the junction nodes. Since we are considering only one junction group (every node contains a $\boldsymbol{b}^{(3)}$ edge), every adjacent node has to have a differing sign because the orientation of the endpoints of each $\boldsymbol{b}^{(3)}$ edge is different. Thus, junction sign definition given by (41) is consistent with the bipartite property as well.

In the next section we consider multiple junctions groups. It will be shown that the ideas developed in this section carry over to that situation and that the presence of different junction groups introduces another level of complexity that can still be simplified by looking at the graph structure of the dislocation network.

7. Graphs of dislocation networks involving all junction groups

When dislocations on all slip systems are involved in junctions all junction groups contribute to the dislocation network. In this case, the bipartite graph concept of a single junction group, which was developed in the previous section can be generalized to a r-partite graph to represent the dislocation network. Here, the number of vertex sets r of such a graph is equal to $2n$, where n is the number of junction types and the factor of 2 represents the different orientations for each group. At the end of Appendix A we show why junction formation in this case retains the r-partite property of the graph. To orient these junction groups we continue to use (41) and refer to this definition as the r-partite coloring. With this definition, when we are only considering one group of junctions, we recover the results obtained in the previous section.

As discussed in the previous section, neighboring nodes in the graph within the same junction group have different orientations (signs). However, this does not guarantee differing signs of nodes on parts of the graph where adjacent nodes have different junction groups. This will have implications for how we convert between the endpoint orientations and each junction group orientation.

Let us now look at the definition of endpoints from the prospective of the graph theoretic ideas, with the goal of illustrating the relationship between the signs of the junction points and endpoints in the case of multiple junction groups. Let us consider the dislocation density tensor on a given slip system as given by (12). Applying the exterior

derivative gives

$$\mathrm{d}\boldsymbol{\alpha}^{(l)} = \mathrm{d}\rho^{(l)}\boldsymbol{b}^{(l)}.$$

We note that $\mathrm{d}\rho^{(l)}$ can be written as a sum containing all the endpoint densities inside the volume which is integrated over. From (8) and (7) , it follows that

$$\mathrm{d}\boldsymbol{\rho}^{(l)} = -\left\langle \sum_{k}^{N^l} T_{\partial c_{\mathrm{o}(k)}^{(l)}} \right\rangle,$$

where $N^{(l)}$ is the number of open lines for a given slip system and $T_{\partial c_{\mathrm{o}}(k)}$ represents the (signed) point Dirac delta function representing an endpoint. Our aim is to model the system using the junction point densities, and since every term in this sum can be identified with one of these junction points (up to a sign), we split this sum into a sum over junction types and a nested sum over the number of points in each type:

$$\begin{aligned}
\mathrm{d}\boldsymbol{\rho}^{(l)} &= -\left\langle \sum_{p,q:\,(lpq)\in S^l} \sum_{i(lpq)} \mathrm{sgn}(\partial c_{\mathrm{o}(i)}^{(l)}) T_{P_{(i)}^{(lpq)}} \right\rangle \\
&= -\left\langle \sum_{p,q:\,(lpq)\in S^l} \sum_{i(lpq)} \mathrm{sgn}^{(lpq,l)} \mathrm{sgn}(P_{(i)}^{(lpq)}) T_{P_{(i)}^{(lpq)}} \right\rangle \\
&= -\sum_{p,q:\,(lpq)\in S^l} \mathrm{sgn}^{(lpq,l)} \left\langle \sum_{i(lpq)} \mathrm{sgn}(P_{(i)}^{(lpq)}) T_{P_{(i)}^{(lpq)}} \right\rangle.
\end{aligned} \tag{46}$$

In this expression S^l is an index set containing all the junction types that slip system l is part of and $i(lpq)$ denotes an index for the sum over all junction nodes which are of type lpq. In the second line the innermost sum is replaced by the junction point currents. This step relies on the fact that every endpoint, $\partial c_{\mathrm{o}(i)}^{(l)}$, can be associated with two other endpoint densities (on other slip systems) to make up the (signed) ith junction point p(i). We have also added $\mathrm{sgn}^{(lpq,l)}$ to convert the junction point orientation (sign) into the endpoint orientation (sign). From (41) we can obtain $\mathrm{sgn}^{(lpq,l)}$ as

$$\mathrm{sgn}^{(lpq,l)} = \frac{1}{\mathrm{sgn}_P(\partial c_{o(i)}^{(p)})\mathrm{sgn}_P(\partial c_{o(i)}^{(q)})} = \mathrm{sgn}_P(\partial c_{o(i)}^{(p)})\mathrm{sgn}_P(\partial c_{o(i)}^{(q)}) \tag{47}$$

We note the dependence on the junction type and slip system (s, l) because the endpoints can be oriented differently relative to adjacent junction groups. We note that $\mathrm{sgn}^{(lpq,l)}$ does not depend on the specific junction point P because, for a given junction group, the relative orientations of the connecting arms are the same. We note here that junction types within the same junction group have the same sign $\mathrm{sgn}^{(lpq,l)}$ because this sign is determined from the Burgers vectors.

With this we can express the endpoint currents in terms of the junction currents as

$$\mathrm{d}\boldsymbol{\rho}^{(l)} = \pi^{(l)} = \sum_{p,q:\,(lpq)\in S^l} \mathrm{sgn}^{(lpq,l)} \pi_{\mathrm{J}}^{(lpq)}, \tag{48}$$

where the junction current is still defined by (42) for each group. When this is represented by smooth forms we obtain

$$\mathrm{d}\boldsymbol{\rho}_{\mathrm{s}}^{(l)} = \pi_s^{(l)} = \sum_{p,q:\,(lpq)\in S^l} \mathrm{sgn}^{(lpq,l)} \pi_{\mathrm{sJ}}^{(lpq)}. \tag{49}$$

The last relationship is viewed as gluing the arms together since in order to arrive at this relationship we had to associate the signs of the endpoint currents to the junction currents. In the above, the signs $\mathrm{sgn}^{(s,l)}$ are determined by the fixing the Burgers vectors of the dislocations. For example, if only two type of junctions are present, which are in different junction groups, and we fixed the Burgers vectors such that

$$\boldsymbol{b}^{(1)} + \boldsymbol{b}^{(2)} + \boldsymbol{b}^{(3)} = 0$$
$$\boldsymbol{b}^{(1)} - \boldsymbol{b}^{(4)} + \boldsymbol{b}^{(5)} = 0,$$

and if the vector density $\boldsymbol{\rho}_s^{(1)}$ has Burgers vector $\boldsymbol{b}^{(1)}$, $\boldsymbol{\rho}_s^{(2)}$ has $\boldsymbol{b}^{(2)}$, and so on, then the index set is $S^1 = \{\{1,2,3\},\{1,4,5\}\}$ and the endpoint density relationships would be:

$$\begin{aligned}
\mathrm{div}\boldsymbol{\rho}_{\mathrm{s}}^{(1)} &= \pi_{\mathrm{sJ}}^{123} - \pi_{\mathrm{sJ}}^{145} \\
\mathrm{div}\boldsymbol{\rho}_{\mathrm{s}}^{(2)} &= \pi_{\mathrm{sJ}}^{123} \\
\mathrm{div}\boldsymbol{\rho}_{\mathrm{s}}^{(3)} &= \pi_{\mathrm{sJ}}^{123} \\
\mathrm{div}\boldsymbol{\rho}_{\mathrm{s}}^{(4)} &= \pi_{\mathrm{sJ}}^{145} \\
\mathrm{div}\boldsymbol{\rho}_{\mathrm{s}}^{(5)} &= -\pi_{\mathrm{sJ}}^{145}.
\end{aligned}$$

Corresponding to this example is the graph shown in Fig.12. In this graph we denote 1 with the color blue, 2 with red, 3 with green, 4 with gold, and 5 with cyan. In that figure, it can be seen that adjacent junction nodes are either of opposite sign or opposite junction group. This property is consistent with r-partite graphs, more specifically a 4-partite graph because the nodes can be split into 4 groups which consist of 2 junction groups each with a positive and negative orientation.

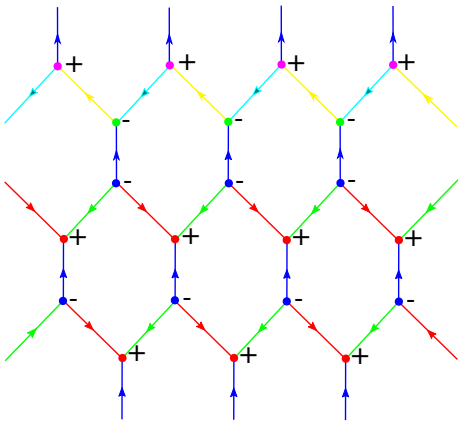

Figure 12: Illustration of the relationship between the signs of the endpoints and junction points for the example in the text. The different color nodes denote the r-partite coloring of the nodes. The corresponding sign is given next to the node.

We end this section by providing a proof that the collinear annihilation preserves the r-partite property of the dislocation network. This reaction is illustrated in Fig. 13, where the reacting dislocations segments e1 and e2

annihilate each other to produce new edges in the graph denoted by e1' and e2'. Looking at the incident vertices v1, v2, v3 and v4, it is possible to identify cases when the nodes (v1,v2) and (v3,v4) are in the same junction group and when they are not. To prove that the annihilation reaction preserves the r-partite property of the graph, let us first consider the case when (v1,v2) and (v3,v4) belong to the same junction group. In this case, it is sufficient to show that the resulting graph is bipartite. Since collinear annihilation amounts to swapping one of the nodes from each edge to another node in the same vertex set, the bipartite property of the graph is preserved. We know that the vertex sets are the same because this is required for the reaction to take place. We note that this process can result in the merging of two previously disconnected components of the graph. When the junction groups are different the r-partite property is trivially preserved because after the reaction v2 and v3 are adjacent and have different junction groups. The same holds for v1 and v4.

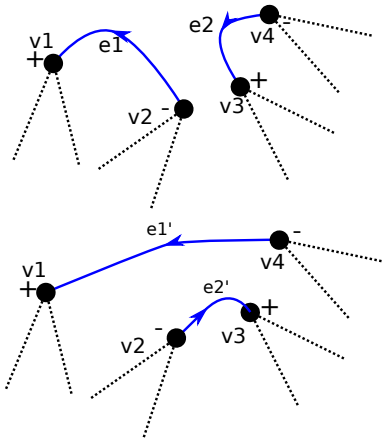

Figure 13: Illustration of collinear annihilation of two dislocation segments in blue before (top) and after the reaction (bottom). The dotted edges signify that these nodes are connected to other nodes that are not shown in the graph.

8. Transport relations for the dislocation network

In this section, the transport equations for the dislocation network are derived. In doing so, we make use of (49), the relationship between the endpoints and the junction points. We state again that the dislocation junction reaction starts out as a crossed state in which two junction points are overlapping then proceeds to form a junction segment via the separation of the two junction points. Here, we will analyze the continuum kinematics associated with open dislocation line segments coupled to the motion of junction points.

8.1. Transport of dislocation lines

Taking the time derivative of (13) gives the transport equation for the vector density of dislocations,

$$\frac{d}{dt}\boldsymbol{\rho}^{(l)} = \left\langle \sum_{k}^{N_{\mathrm{c}}^{(l)}} \frac{d}{dt} T_{c_{\mathrm{c}(k)}^{(l)}} + \sum_{n}^{N_{\mathrm{o}}^{(l)}} \frac{d}{dt} T_{c_{\mathrm{o}(n)}^{(l)}} \right\rangle. \tag{50}$$

As the equation indicates, the dislocation population is assumed to have both closed and open lines. The summand in the first summation above is given by

$$\frac{d}{dt}T_{c^{(l)}_{\mathrm{c}(k)}} = -\mathrm{d}\,\mathrm{i}_{\boldsymbol{v}|_{c^{(l)}_{\mathrm{c}(k)}}}T_{c^{(l)}_{\mathrm{c}(k)}}, \tag{51}$$

where use has been made of Lie derivative relation (11) and the fact that $\partial c^{(l)}_{\mathrm{c}(k)} = \emptyset$ for closed lines. In this result, the current $\mathrm{i}_{\boldsymbol{v}|_{c^{(l)}_{\mathrm{c}(k)}}}T_{c^{(l)}_{\mathrm{c}(k)}}$ represents the rate of increment in slipped area due to the movement of closed lines. In the time evolution of the current induced by open line segments, an extra term emerges which represents the line created by dragging the endpoint of the lines. Accounting for the fact that $\mathrm{d}T_{c_{\mathrm{c}(k)}} = (-1)^{p+1}T_{\partial c_{\mathrm{c}(k)}}$, we may then write

$$\frac{d}{dt}T_{c^{(l)}_{\mathrm{o}(n)}} = -\mathrm{d}\,\mathrm{i}_{\boldsymbol{v}^{(l)}|_{c^{(l)}_{\mathrm{o}(n)}}}\mathrm{T}_{c^{(l)}_{\mathrm{o}(n)}} + \mathrm{i}_{\boldsymbol{v}^{(l)}|_{\partial c^{(l)}_{\mathrm{o}(n)}}}\mathrm{T}_{\partial \mathrm{c}^{(l)}_{\mathrm{o}(n)}}. \tag{52}$$

Again, use has been made of Lie derivative relation (11). In the last expression the velocity evaluated at the endpoint of the open line is denoted by $\boldsymbol{v}^{(l)}|_{\partial c^{(l)}_{\mathrm{o}(n)}}$ while the velocity along the bulk part of the line is denoted by $\boldsymbol{v}^{(l)}|_{c^{(l)}_{\mathrm{o}(n)}}$. Substituting (51) and (52) into (50) and using the fact that the exterior derivative commutes with ensemble averaging yields

$$\frac{d}{dt}\boldsymbol{\rho}^{(l)} = -\mathrm{d}\left\langle\sum_{k}^{N^{(l)}_{\mathrm{c}}}\mathrm{i}_{\boldsymbol{v}^{(l)}|_{c^{(l)}_{\mathrm{c}(k)}}}T_{c^{(l)}_{\mathrm{c}(k)}} + \sum_{n}^{N^{(l)}_{\mathrm{o}}}\mathrm{i}_{\boldsymbol{v}^{(l)}|_{c^{(l)}_{\mathrm{o}(n)}}}T_{c^{(l)}_{\mathrm{o}(n)}}\right\rangle + \left\langle\sum_{n}^{N^{(l)}_{\mathrm{o}}}\mathrm{i}_{\boldsymbol{v}^{(l)}|_{\partial c^{(l)}_{\mathrm{o}(n)}}}T_{\partial c^{(l)}_{\mathrm{o}(n)}}\right\rangle \tag{53}$$

for the evolution of the slip system dislocation current $\boldsymbol{\rho}^{(l)}$.

We note that the interior multiplication with respect to the dislocation velocity $\boldsymbol{v}_k$ of the kth dislocation does not commute with the ensemble average unless all dislocations contributing to the local density share (almost) the same direction (Hochrainer, 2007), as in the line bundle approximation. In this case also the velocity vectors share the same direction and an average velocity vector $\bar{\boldsymbol{v}}$ may be defined, which enters the interior multiplication within the ensemble average.

Since we are representing the dislocation network in terms of the junction point densities, we convert the endpoint currents to junction point currents via: $-T_{\partial c^{l}_{o(j)}} = \mathrm{sgn}^{(lpq,l)}\mathrm{sgn}(P^{(lpq)}_{(j)})T_{P^{(lpq)}_{(j)}}$. We further introduce a junction constraint on the endpoint velocities in (53) so that each of the connecting arms at the junction point move together at the speed of the junction point itself, $\boldsymbol{v}^{(lpq)}_{\mathrm{J}(n)}$. Moreover, we assume that an ensemble average velocity field can be defined for the junction points. Note that the junction point velocities are in general not perpendicular to the line direction. The junction points are, however, usually restricted to move along intersection lines of slip systems. The average junction point velocity shall be denoted with $\bar{\boldsymbol{v}}^{(lpq)}_{\mathrm{J}}$. With currents being represented by smooth forms, these steps lead to the following evolution law for the dislocation density:

$$\frac{d}{dt}\boldsymbol{\rho}_{\mathbf{s}}{}^{(l)} = -\mathrm{d}\,\mathrm{i}_{\bar{\boldsymbol{v}}^{(l)}}\boldsymbol{\rho}^{(l)}_{\mathrm{s}} - \sum_{p,q:\,(lpq)\in S^{l}}\mathrm{sgn}^{(lpq,l)}\mathrm{i}_{\bar{\boldsymbol{v}}^{(lpq)}_{\mathrm{J}}}\boldsymbol{\pi}^{(lpq)}_{\mathrm{sJ}}, \tag{54}$$

where the convention that the smooth endpoint densities are positive at the start of the line has been used. When written using vector calculus notion for vectors fields in R^3 (given a Euclidean metric) (Lee, 2013, p. 368) the last equations reads

$$\frac{d}{dt}\boldsymbol{\rho}^{(l)}_{\mathrm{s}} = \mathrm{curl}\left(\bar{\boldsymbol{v}}^{(l)}\times\boldsymbol{\rho}^{(l)}_{\mathrm{s}}\right) - \sum_{p,q:\,(lpq)\in S^{l}}\mathrm{sgn}^{(lpq,l)}\bar{\boldsymbol{v}}^{(lpq)}_{\mathrm{J}}\boldsymbol{\pi}^{(lpq)}_{\mathrm{sJ}}. \tag{55}$$

The first term in (55) accounts for the transport of the dislocation lines while the second term reflects the movement of the junction points. Note that setting the junction point velocity to zero produces Frank-Read type multiplication (Weger and Hochrainer, 2019), while the motion of the junction points would leave the kinematics of the dislocation 'unaffected' if the junction point velocity equals the dislocation velocity. Finding suitable constitutive assumptions for the junction point velocity is yet an open topic.

It is now possible to cast the evolution model of the dislocations on a given slip system in terms of a single dislocation density and two junction density measures for each junction group, one for the positive junction points and one for the negative junction points. In this case, arguments similar to which allowed us to arrive at (55) can be used to write

$$\frac{d}{dt}\boldsymbol{\rho}_{\mathrm{s}}^{(l)} = \operatorname{curl}\left(\overline{\boldsymbol{v}}^{(l)} \times \boldsymbol{\rho}_{\mathrm{s}}^{(l)}\right) - \sum_{p,q:\,(lpq)\in S^{l}} \operatorname{sgn}^{(lpq,l)}\left(\overline{\boldsymbol{v}}_{\mathrm{J}}^{(lpq)+}\pi_{\mathrm{sJ}}^{(lpq)+} - \overline{\boldsymbol{v}}_{\mathrm{J}}^{(lpq)-}\pi_{\mathrm{sJ}}^{(lpq)-}\right). \tag{56}$$

In the above, we have grouped junction densities according to their sign and the sign of the negative junction point density has been explicitly taken into account by the minus sign. The reaction term in (56) is fundamentally different from similar terms added in previous CDD models (Lin and El-Azab, 2020; Sudmanns et al., 2020) where such terms were cast as products of the reacting densities.

8.2. Transport of junction point densities

Next, we provide transport relations for the junction point density and the associated positive and negative junction point densities. From their definitions in (42), these densities represent signed zero currents and will be treated as such in the following derivations. Taking the time derivative of (42) combined with the Lie derivative relation (11), considering that zero dimensional currents have no boundary, and that the exterior derivative commutes with averaging we obtain

$$\frac{d}{dt}\pi_{\mathrm{J}}^{(pqr)} = -\mathrm{d}\left\langle \sum_{n} i_{\boldsymbol{v}_{J(n)}^{(pqr)}} \operatorname{sgn}(P_{(n)}^{(pqr)}) T_{P_{(n)}^{(pqr)}} \right\rangle. \tag{57}$$

When the currents are represented by smooth forms the closed form of the equation becomes

$$\frac{d}{dt}\pi_{\mathrm{sJ}}^{(pqr)} = -\mathrm{d}\,\mathrm{i}_{\overline{\boldsymbol{v}}_{\mathrm{J}}^{(pqr)}}\pi_{\mathrm{sJ}}^{(pqr)}, \tag{58}$$

with $\overline{\boldsymbol{v}}_{\mathrm{J}}^{(pqr)}$ denoting the average velocity of junction points. In terms of vector calculus operations acting on the corresponding vector fields in R^3 (given an Euclidean metric) (Lee, 2013, p. 368) we can write the last equation in the form

$$\frac{d}{dt}\pi_{\mathrm{sJ}}^{(pqr)} = -\operatorname{div}\left(\overline{\boldsymbol{v}}_{\mathrm{J}}^{(pqr)}\pi_{\mathrm{sJ}}^{(pqr)}\right). \tag{59}$$

For the reasons described in section 5 we decide to describe the dislocation network using positive and negative junction densities. When dislocations react and form glissile junctions, two junction points are created with opposite orientations. To model this, source terms are added to the transport equations for the positive and negative junction

densities. Using arguments similar to those that led to (59) we arrive at

$$\begin{aligned}\frac{d}{dt}\pi_{\mathrm{sJ}}^{(pqr)+} &= -\mathrm{div}\left(\bar{\boldsymbol{v}}_{\mathrm{J}}^{(pqr)+}\pi_{\mathrm{s}}^{(pqr)+}\right) + S^{+} \\ \frac{d}{dt}\pi_{\mathrm{sJ}}^{(pqr)-} &= -\mathrm{div}\left(\bar{\boldsymbol{v}}_{\mathrm{J}}^{(pqr)-}\pi_{\mathrm{s}}^{(pqr)-}\right) + S^{-}.\end{aligned} \tag{60}$$

We note that $\pi_{\mathrm{sJ}}^{pqr} = \pi_{\mathrm{sJ}}^{(pqr)+} - \pi_{\mathrm{sJ}}^{(pqr)-}$, with $\pi^{(pqr)+}$ and $\pi^{(pqr)-}$ being positive scalars, and thus $\dot{\pi}_{sJ}^{pqr} = \dot{\pi}_{\mathrm{sJ}}^{(pqr)+} - \dot{\pi}_{\mathrm{sJ}}^{(pqr)-}$. From this we find that we must require, $\bar{\boldsymbol{v}}_{\mathrm{J}}^{(pqr)}\pi_{s}^{(pqr)} = \bar{\boldsymbol{v}}_{J}^{(pqr)+}\pi_{\mathrm{s}}^{(pqr)+} - \bar{\boldsymbol{v}}_{\mathrm{J}}^{(pqr)-}\pi_{\mathrm{s}}^{(pqr)-}$, which we could interpret as a definition of the mean signed point density velocity $\bar{\boldsymbol{v}}_{J}^{(pqr)}$, and $S^{+} = S^{-} = S$. To summarize, the dislocation network evolution can be described in terms of the evolution laws (56) and (60):

$$\begin{aligned}\frac{d}{dt}\boldsymbol{\rho}_{\mathrm{s}}^{(l)} &= \mathrm{curl}\left(\bar{\boldsymbol{v}}^{(l)} \times \boldsymbol{\rho}_{\mathrm{s}}^{(l)}\right) - \sum_{p,q:\,(lpq)\in S^{l}} \mathrm{sgn}^{(lpq,l)}\left(\bar{\boldsymbol{v}}_{\mathrm{J}}^{(lpq)+}\pi_{\mathrm{sJ}}^{(lpq)+} - \bar{\boldsymbol{v}}_{\mathrm{J}}^{(lpq)-}\pi_{\mathrm{sJ}}^{(lpq)-}\right) \\ \frac{d}{dt}\pi_{\mathrm{sJ}}^{(pqr)+} &= -\mathrm{div}\left(\bar{\boldsymbol{v}}_{\mathrm{J}}^{(pqr)+}\pi_{\mathrm{sJ}}^{(pqr)+}\right) + S \\ \frac{d}{dt}\pi_{\mathrm{sJ}}^{(pqr)-} &= -\mathrm{div}\left(\bar{\boldsymbol{v}}_{\mathrm{J}}^{(pqr)-}\pi_{\mathrm{sJ}}^{(pqr)-}\right) + S.\end{aligned} \tag{61}$$

For completeness, we also introduce the transport relations for the virtual segments which are given in the form

$$\frac{d}{dt}\boldsymbol{\rho}_{\mathrm{v,s}}^{(l)} = \sum_{p,q:\,(lpq)\in S^{l}} \mathrm{sgn}^{(lpq,l)}\left(\bar{\boldsymbol{v}}_{\mathrm{J}}^{(lpq)+}\pi_{\mathrm{sJ}}^{(lpq)+} - \bar{\boldsymbol{v}}_{\mathrm{J}}^{(lpq)-}\pi_{\mathrm{sJ}}^{(lpq)-}\right) \tag{62}$$

These equations represent the fact that the virtual segments only grow due to movement of junction points which they are attached to. We note that modeling the evolution of the density of virtual segments is not necessary to describe the transport of the system given by (61), because this evolution is equivalent to the transport of the endpoint densities.

9. Dislocation reactions as source terms

The evolution laws (61) do not describe the reaction process itself, i.e, the change in the topology of the dislocation network associated with the creation of new junction points. This a task requires the specification of the source term S introduced in the transport equations for the positive and negative junction point densities in (60) and (61). In the discrete dislocation dynamics (DDD) literature, these processes are referred to as node merging and node splitting. The goal of this section is to incorporate this type of information into the transport equations (61). In doing so, we use the notion of transversal intersections to get a measure of when dislocations intersect.

Geometrically, the formation of junctions starts with the intersection of two lines and the creation of two overlapping junction nodes, as detailed in Bulatov et al. (2006). An important issue here is to quantify the intersection of two lines in R^3. The machinery of transversal intersections can help in this regard but we are faced with the fact that the transversal intersection depends on the ambient space (Guillemin and Pollack, 2010), which makes it difficult to define the intersection between two lines in R^3. It is, however, easier to define the transversal intersection of the surfaces swept by two dislocations due to their motion in four-dimensional space-time. This intersection corresponds to the cutting of dislocations and thus gives a measure of how many dislocation-dislocation reactions occur.

To determine the rate of dislocation cutting we introduce a zero-dimensional space-time current $\mathcal{T}_{\pitchfork}$, which yields a 4-form, i.e., a rate of volume density, upon averaging. This current is defined from the space-time surfaces (world sheets) drawn by the dislocations. Let the dislocation c_t for every time $t \in [0, T)$ be parametrized by some parameter $s \in [0, S)$, such that $c_t = \{c_t(s), s \in [0, S)\}$. Then the space-time surface of the moving dislocation is a two-dimensional submanifold Σ of 4D space-time, which is parametrized by

$$\Sigma(s, t) = (t, c_t(s)). \tag{63}$$

Let $\Sigma_j^{(k)}$ be the space-time surface of dislocation $c_j^{(k)}$, then to get a measure of dislocation-dislocation cutting we define the space-time current

$$\mathcal{T}_{\pitchfork}^{(l,k)}[\theta] \equiv \left\langle \sum_{i \in N^{(l)}, j \in N^{(k)}} \mathcal{T}_{\Sigma_i^{(l)} \pitchfork \Sigma_j^{(k)}}[\theta] \right\rangle,$$

where $\Sigma_i^{(l)} \pitchfork \Sigma_j^{(k)}$ denotes the transversal intersection of the two space-time surfaces. The restriction to transversal intersections excludes intersections of dislocations which move on the same glide plane, because the intersection of their world-sheets would be a curve in space-time. For the transversal case we depict the intersection of two world sheets by projecting the 4D space-time manifolds onto 3D space in Fig. 14. Note that while the spatial surfaces swept by the two dislocations intersect along a line, the curves only actually met each other at a given point in time, indicated by the blue dot in the figure. Transversal intersection in space-time yields this point in space-time, which combines the spatial position and the time of encounter. The transversal intersection of the submanifolds which induce the current $\mathcal{T}_{\pitchfork}^{(l,k)}$ corresponds to the exterior product of the currents induced by the involved submanifolds, i.e.,

$$\mathcal{T}_{\pitchfork}^{(l,k)} = \left\langle \sum_{i \in N^{(l)}, j \in N^{(k)}} \mathcal{T}_{\Sigma_i^{(l)}} \wedge \mathcal{T}_{\Sigma_j^{(k)}} \right\rangle . \tag{64}$$

Ensemble averaging then yields a smooth differential 4-form, $\Gamma_{\mathrm{s}}^{(l,k)}$, such that $\mathcal{T}_{\pitchfork}^{(l,k)}[\theta] = \mathcal{T}_{\Gamma_{\mathrm{s}}^{(l,k)}}[\theta]$.

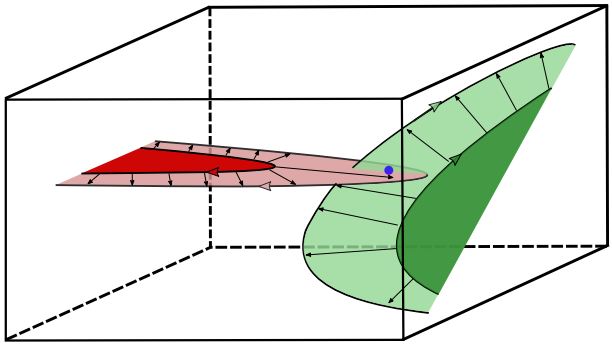

Figure 14: Intersection of dislocation worldsheets projected onto three dimensional space. The intersection point of the corresponding worldsheets in 4D space is projected onto the blue point in the figure.

In general, the dislocation positions and their velocities on the involved slip systems will be correlated and the average of the product currents in (64) will not be the product of the average currents but contain additional correlation

information. Such correlation information may in principle be obtained from DDD simulations. However, no such information is currently available and therefore we shall assume the space-time sheets to be uncorrelated, such that

$$\mathcal{T}^{(l,k)}_{\pitchfork} = \left\langle \sum_{i\in N^{(l)}} \mathcal{T}_{\Sigma^{(l)}_i} \right\rangle \wedge \left\langle \sum_{j\in N^{(k)}} \mathcal{T}_{\Sigma^{(k)}_j} \right\rangle. \tag{65}$$

The space-time currents on the right hand side are due to the line-density assumption and by definition of the average velocity given by

$$\left\langle \sum_{i\in N^{(l)}} \mathcal{T}_{\Sigma^{(l)}_i} \right\rangle = \mathrm{i}_{(1,\bar{\boldsymbol{v}}^{(l)})}\mathrm{i}_{(0,\boldsymbol{\rho}_{\mathrm{s}}{}^{(l)})}\mathrm{d}V_t = \mathrm{i}_{\boldsymbol{\rho}_{\mathrm{s}}{}^{(l)}}\mathrm{d}V + \left(\mathrm{i}_{\bar{\boldsymbol{v}}^{(l)}}\mathrm{i}_{\boldsymbol{\rho}_{\mathrm{s}}{}^{(l)}}\mathrm{d}V\right)\wedge \mathrm{d}t, \tag{66}$$

where $\mathrm{d}V_t = \mathrm{d}V \wedge \mathrm{d}t$ is the space-time volume form and the space time velocity $\mathcal{V} = (1, \boldsymbol{v}^{(l)})$ has unit speed in time direction, while the time-component of the space-time dislocation density vanishes. The smooth 4-form $\Gamma^{(l,k)}_{\mathrm{s}}$ corresponding to the average current (65) is accordingly given by

$$\begin{aligned}
\Gamma^{(l,k)}_{\mathrm{s}} &= \left[\mathrm{i}_{\boldsymbol{\rho}^{(l)}_{\mathrm{s}}}\mathrm{d}V + \left(\mathrm{i}_{\bar{\boldsymbol{v}}^{(l)}}\mathrm{i}_{\boldsymbol{\rho}^{(l)}_{\mathrm{s}}}\mathrm{d}V\right)\wedge \mathrm{d}t\right] \wedge \left[\mathrm{i}_{\boldsymbol{\rho}^{(k)}_{\mathrm{s}}}\mathrm{d}V + \left(\mathrm{i}_{\bar{\boldsymbol{v}}^{(k)}}\mathrm{i}_{\boldsymbol{\rho}^{(k)}_{\mathrm{s}}}\mathrm{d}V\right)\wedge \mathrm{d}t\right] \\
&= \left[\boldsymbol{\rho}^{(l)}_{\mathrm{s}}\cdot\left(\boldsymbol{\rho}^{(k)}_{\mathrm{s}}\times\bar{\boldsymbol{v}}^{(k)}\right) + \boldsymbol{\rho}^{(k)}_{\mathrm{s}}\cdot\left(\boldsymbol{\rho}^{(l)}_{\mathrm{s}}\times\bar{\boldsymbol{v}}^{(l)}\right)\right]\mathrm{d}V_t \\
&= \left(\boldsymbol{\rho}^{(l)}_{\mathrm{s}}\times\boldsymbol{\rho}^{(k)}_{\mathrm{s}}\right)\cdot\left(\bar{\boldsymbol{v}}^{(k)} - \bar{\boldsymbol{v}}^{(l)}\right)\mathrm{d}V_t.
\end{aligned} \tag{67}$$

The 4-form $\Gamma^{(l,k)}_{\mathrm{s}}$ defines the rate of signed intersections between two slip systems, when dislocations on the slip systems move independently of each other and remain unaffected by the intersections. A very preliminary investigation on non-linearities which would emerge from considering the mutual intersections in the dislocation velocities has been provided in Hochrainer et al. (2008). In the current work we consider the interactions of the slip systems by assuming that a certain fraction of the encounters yield junction points. This fraction may be determined from reaction maps available from discrete dislocation studies (Kubin et al., 2003; Weygand and Gumbsch, 2005). The propensity of two intersecting dislocations to form a junction strongly depends on the relative orientation of dislocations. However, we shall suppress this dependency in the following notation and assume reaction coefficients $R^{(l,k)}$ given. The creation rate of junction points between slip systems is then given by

$$\bar{S}^{(l,k)} = R^{(l,k)}\left(\boldsymbol{\rho}^{(l)}_{\mathrm{s}}\times\boldsymbol{\rho}^{(k)}_{\mathrm{s}}\right)\cdot\left(\bar{\boldsymbol{v}}^{(k)} - \bar{\boldsymbol{v}}^{(l)}\right). \tag{68}$$

We note that since the intersection rate was defined using the notion of a transversal intersection it does not give a measure of reactions when dislocations (and their velocities) are coplanar or when the line directions are parallel, i.e. if $\boldsymbol{\rho}^{(k)}_{\mathrm{s}}\times\boldsymbol{\rho}^{(l)}_{\mathrm{s}} = 0$. Due to the signed nature of this measure, we also encounter cancellations when using it at increasing scales.

We now introduce the source term for the positive and negative junction points into the transport relations (61),

which now read

$$\begin{aligned}
\frac{d}{dt}\boldsymbol{\rho}_{\mathrm{s}}^{(l)} &= \operatorname{curl}\left(\bar{\boldsymbol{v}}^{(l)} \times \boldsymbol{\rho}_{\mathrm{s}}^{(l)}\right) - \sum_{p,q:\,(lpq)\in S^l} \operatorname{sgn}^{(lpq,l)}\left(\bar{\boldsymbol{v}}_{\mathrm{J}}^{(lpq)+}\pi_{\mathrm{sJ}}^{(lpq)+} - \bar{\boldsymbol{v}}_{\mathrm{J}}^{(lpq)-}\pi_{\mathrm{sJ}}^{(lpq)-}\right) \\
\frac{d}{dt}\pi_{\mathrm{sJ}}^{(p)+} &= -\operatorname{div}\left(\bar{\boldsymbol{v}}_{\mathrm{J}}^{(p)+}\pi_{\mathrm{sJ}}^{(p)+}\right) + \sum_{j\in I^p} \bar{S}^{(p,j)} \\
\frac{d}{dt}\pi_{\mathrm{sJ}}^{(p)-} &= -\operatorname{div}\left(\bar{\boldsymbol{v}}_{\mathrm{J}}^{(p)-}\pi_{\mathrm{sJ}}^{-(p)}\right) + \sum_{j\in I^p} \bar{S}^{(p,j)}.
\end{aligned} \tag{69}$$

In the above, $\bar{S}^{(s,j)}$ is obtained from (68) and I^p is an index set containing the number of unique pairs of slip systems that react to form the junction type associated to $\pi^{(p)}$.

We now give an explicit example for the case of 3 slip systems and only 1 junction type with Burgers vector fixed such that $\boldsymbol{b}^{(1)} + \boldsymbol{b}^{(2)} - \boldsymbol{b}^{(3)} = 0$. In this case, the evolution equations for the dislocation densities read:

$$\begin{aligned}
\frac{d}{dt}\boldsymbol{\rho}_{\mathrm{s}}^{(1)} &= \operatorname{curl}\left(\bar{\boldsymbol{v}}^{(1)} \times \boldsymbol{\rho}_{\mathrm{s}}^{(1)}\right) - \left(\bar{\boldsymbol{v}}_{\mathrm{J}}^{+(123)}\pi_{\mathrm{sJ}}^{(123)+} - \bar{\boldsymbol{v}}_{\mathrm{J}}^{(123)-}\pi_{\mathrm{sJ}}^{(123)-}\right) \\
\frac{d}{dt}\boldsymbol{\rho}_{\mathrm{s}}^{(2)} &= \operatorname{curl}\left(\bar{\boldsymbol{v}}^{(2)} \times \boldsymbol{\rho}_{\mathrm{s}}^{(2)}\right) - \left(\bar{\boldsymbol{v}}_{\mathrm{J}}^{(123)+}\pi_{\mathrm{sJ}}^{(123)+} - \bar{\boldsymbol{v}}_{\mathrm{J}}^{-(123)}\pi_{\mathrm{sJ}}^{(123)-}\right) \\
\frac{d}{dt}\boldsymbol{\rho}_{\mathrm{s}}^{(3)} &= \operatorname{curl}\left(\bar{\boldsymbol{v}}^{(3)} \times \boldsymbol{\rho}_{\mathrm{s}}^{(3)}\right) + \left(\bar{\boldsymbol{v}}_{\mathrm{J}}^{(123)+}\pi_{\mathrm{sJ}}^{(123)+} - \bar{\boldsymbol{v}}_{\mathrm{J}}^{-(123)}\pi_{\mathrm{sJ}}^{(123)-}\right),
\end{aligned} \tag{70}$$

and those for the junction point densities read:

$$\begin{aligned}
\frac{d}{dt}\pi_{\mathrm{sJ}}^{(123)+} &= -\operatorname{div}\left(\bar{\boldsymbol{v}}_{\mathrm{J}}^{(123)+}\pi_{\mathrm{sJ}}^{(123)+}\right) \\
&\quad + R^{(1,2)}\left(\boldsymbol{\rho}_{s}^{(2)} \times \boldsymbol{\rho}_{s}^{(1)}\right)\cdot \boldsymbol{v}_{\mathrm{rel}}^{(1,2)} + R^{(3,1)}\left(\boldsymbol{\rho}_{\mathrm{s}}^{(3)} \times \boldsymbol{\rho}_{\mathrm{s}}^{(1)}\right)\cdot \boldsymbol{v}_{\mathrm{rel}}^{(1,3)} + R^{(3,2)}\left(\boldsymbol{\rho}_{\mathrm{s}}^{(3)} \times \boldsymbol{\rho}_{\mathrm{s}}^{(2)}\right)\cdot \boldsymbol{v}_{\mathrm{rel}}^{(2,3)} \\
\frac{d}{dt}\pi_{\mathrm{sJ}}^{(123)-} &= -\operatorname{div}\left(\bar{\boldsymbol{v}}_{\mathrm{J}}{}^{(123)-}\pi_{\mathrm{sJ}}^{(123)-}\right) \\
&\quad + R^{(1,2)}\left(\boldsymbol{\rho}_{\mathrm{s}}^{(2)} \times \boldsymbol{\rho}_{\mathrm{s}}^{(1)}\right)\cdot \boldsymbol{v}_{\mathrm{rel}}^{(1,2)} + R^{(3,1)}\left(\boldsymbol{\rho}_{\mathrm{s}}^{(3)} \times \boldsymbol{\rho}_{\mathrm{s}}^{(1)}\right)\cdot \boldsymbol{v}_{\mathrm{rel}}^{(1,3)} + R^{(3,2)}\left(\boldsymbol{\rho}_{\mathrm{s}}^{(3)} \times \boldsymbol{\rho}_{\mathrm{s}}^{(2)}\right)\cdot \boldsymbol{v}_{\mathrm{rel}}^{(2,3)}.
\end{aligned} \tag{71}$$

We end this section with a test simulation illustrating the role of the source terms in the dislocation density evolution equation (61), which is tied to the transport of the junction point densities. In the 3-slip system case shown in equation (70) and (71), we simulate the evolution of the dislocation density of one slip system by suppressing the transport part and activating the junction point transport part. Since we only simulate one vector density, the reaction terms are eliminated from the positive and negative junction transport equations, which then simplify to:

$$\begin{aligned}
\frac{d}{dt}\boldsymbol{\rho}_{\mathrm{s}}^{(1)} &= -\left(\bar{\boldsymbol{v}}_{\mathrm{J}}^{+(123)}\pi_{\mathrm{sJ}}^{(123)+} - \bar{\boldsymbol{v}}_{\mathrm{J}}^{(123)-}\pi_{\mathrm{sJ}}^{(123)-}\right) \\
\frac{d}{dt}\pi_{\mathrm{sJ}}^{(123)+} &= -\operatorname{div}\left(\bar{\boldsymbol{v}}_{\mathrm{J}}^{(123)+}\pi_{\mathrm{sJ}}^{(123)+}\right) \\
\frac{d}{dt}\pi_{\mathrm{sJ}}^{(123)-} &= -\operatorname{div}\left(\bar{\boldsymbol{v}}_{\mathrm{J}}^{(123)-}\pi_{\mathrm{sJ}}^{(123)-}\right).
\end{aligned}$$

We start by initializing overlapping positive and negative junction point densities in the center of the simulation domain and a zero initial value of the simulated dislocation density. We specify a junction point velocity field that separates positive and negative junction point densities apart along the y-axis such that a dislocation junction segment

is created between them. The positive and negative junction point velocities are then reversed and the junction segment between the two densities is gradually erased as the junction densities approach each other. A first-order system least-squares (FOSLS) finite element method with an implicit Euler time integrator was used to discretize the system in space and time. Fig. 15 shows a line profile of the evolution of the dislocation density and the junction point densities along the y-axis. In this figure, we notice some numerical diffusion of the junction point densities, which is expected with the use of implicit Euler time integrator with no diffusion correction. Even with this numerical diffusion, the junction densities are still conserved during the evolution and can still completely remove the junction segment after the junction point velocities are fully reversed.

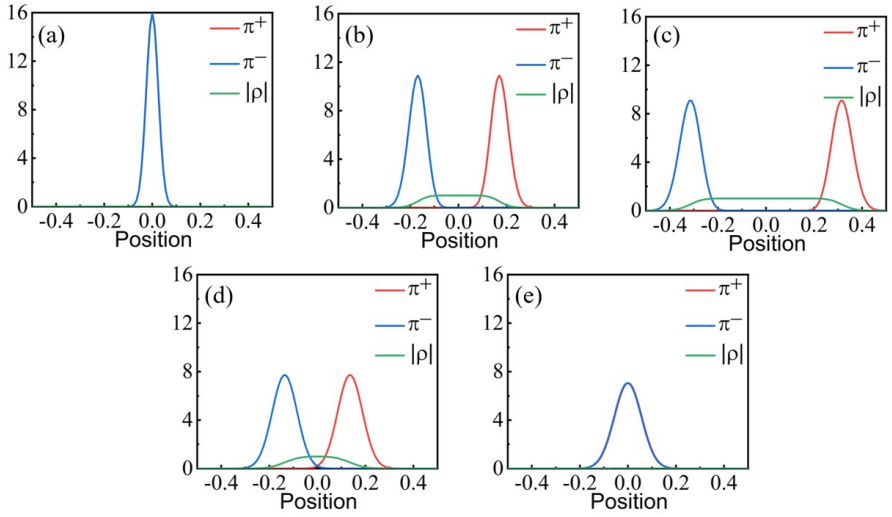

Figure 15: Evolution of the dislocation density and the positive and negative junction point densities along the y-axis of the simulation domain. As the system evolves from its initial conditions (a) to subsequent configurations (b) through (e), the junction points initially move away from each other in (a)-(c), drawing out a junction segment. Then the junction velocities are reversed starting at (c) and the junction segment is gradually erased as the junction point densities move closer until the process is completed in (e).

10. Concluding remarks

A novel representation of complex dislocation configurations in FCC crystals has been established by viewing dislocation configurations as networks consisting of dislocation lines ending at junction points. In addition to the dislocation density, the junction point densities were introduced as kinematic variables of the dislocation network. Graph theory was used to investigate the connectivity of the dislocation network and establish a connection between endpoints and junction points for open dislocation lines. The concept of de Rham currents along with ensemble averaging were used to derive the evolution laws for the dislocation and junction point densities. These laws comprise the transport-reaction equations for the dislocation density and junction point densities which are coupled via source terms arising from the transport of junction points and intersections of dislocations.

It was shown that the integral relation $\int_F \boldsymbol{\alpha} = \int_{\partial F} \boldsymbol{\beta}^p$ can be recovered with the help of Frank's second rule along with the use of virtual dislocation segments. It was also found that the graph representing the dislocation network

under the condition of glissile junction formation is a r-partite multigraph and that the collinear annihilation reaction of dislocations does not destroy this property. These findings were used to establish a relationship between the line endpoint and junction points, which was crucial in writing the final form for the transport relations of the relevant densities. In addition, the use of the concept of transversal intersections made it possible to define a measure of dislocation reactions leading to junction formation. This measure was essential in defining the source terms in the evolution laws for the junction point densities.

From a geometric standpoint, the introduction of end and junction point densities and open line densities is intuitive and naturally represents topological information of the dislocation network. This opens the way to modify current continuum dislocation dynamics frameworks, which are mostly based upon dislocation line information. The introduction of the junction points can also enable the use of graph theory ideas to analyze complex dislocations networks where information about lines and nodes is important in the constitutive behavior of the dislocation systems.

In developing the current framework for handling the kinematics of complex dislocation configurations, glissile junction reactions were considered in illustrating the basic ideas. However, the final form of the evolution laws of the dislocation and junction point densities are valid when other reactions such cross slip, annihilation reactions, and sessile junction formation are allowed. The properties of the associated graphs in these cases require further investigation.

The introduction of junction point densities enables us to define an edge number density of the open dislocation lines. We have shown this in Appendix B. This information could then be used to construct an average link length density (at no additional cost) which is shown to be a useful quantity (Sills et al., 2018) in characterizing the network.

The current work on modeling dislocation network kinematics is preliminary and is still at the conceptual stage. However, the principal step to move from line information to combined line and point information, i.e., from planar closed dislocation curves to planar segments, holds the promise to incorporate salient topological information into the largely geometric dislocation density descriptions used in continuum dislocation theories. For developing an actual continuum theory of evolving dislocation networks there are still major open questions to be answered. Still on the kinematic level, for example, the connectivity between dislocations and junction points was in the current work established in the line density approximation by introducing the junction point densities. But when the averaging volume additionally contains statistically stored dislocations on each slip system, this connection will only be given in a statistical sense. One avenue for dealing with this may be to again resort to the higher dimensional description in orientation space (Hochrainer, 2007), where the endpoints still carry the line orientation information. The higher dimensional end- or junction point density could then likewise be projected to alignment tensors in physical space. Directional differences between the segments involved in junctions would be expected to yield a generalization of curvature variables. The latter have been recently connected to orientation changes in evaluating straight segment based upon DDD simulations Weger et al. (2021). The curvature variables (Hochrainer, 2007) carry some topological information in the case without junctions. If and in case how this information is connected to the topological information of graph theory will be one of the key questions for developing a general continuum description of dislocation

networks. However, in order to describe evolving networks, reaction kinetics, as well as junction and junction point mobilities will be needed. Specifically, the driving forces for junction node motion must be developed and connected with the junction node velocity. Statistical information on reactions has already been successfully incorporated in continuum dislocation descriptions (Stricker et al., 2018; Lin and El-Azab, 2020; Vivekanandan et al., 2021), but for obvious reasons they have not yet been connected to the newly introduced junction point densities, their creation, destruction, or motion. This will require novel approaches to evaluating dynamic information from DDD simulations.

Acknowledgements

This research was supported by the National Science Foundation, Division of Civil, Mechanical, and Manufacturing Innovation (CMMI) through award number 1663311 at Purdue University. The authors appreciate the useful comments by the referees, which led to improvement of the manuscript.

Appendix A. Graph formation argument

In section 6, it was mentioned that the graph representing a single junction group is bipartite under the rule that a dislocation can only react with a single arm of a junction. This is a topological requirement dictated by the physics of junction formation. Fig. 8 shows a typical graph for this case. In this appendix, we clarify how this topological requirement arises. In section 7, the case of multiple junction groups was also considered. In this case, the graph representing the dislocation network was said to be r-partite. It will be shown in this appendix that, in this case, a dislocation can react with more than one arm of the junction node without altering the r-partite characteristic of the graph.

We start with the case of a single junction group. With Burgers vectors fixed as given in Table 1 the corresponding junction reactions at each node in the corresponding graph must be given in the form (modulo a sign)

$$\begin{aligned} \boldsymbol{b}_2 + \boldsymbol{b}_6 - \boldsymbol{b}_3 &= 0 \\ \boldsymbol{b}_3 + \boldsymbol{b}_5 - \boldsymbol{b}_1 &= 0 \\ \boldsymbol{b}_2 + \boldsymbol{b}_5 - \boldsymbol{b}_4 &= 0 \\ \boldsymbol{b}_4 + \boldsymbol{b}_6 - \boldsymbol{b}_1 &= 0. \end{aligned} \tag{A.1}$$

The set of Burgers vectors in Table 1 can be represented geometrically as edges of a tetrahedron, see Fig. A.16. The equations above thus correspond to the reactions formed by considering Burgers vector on the individual faces of the tetrahedron. Junctions resulting from such reactions are called coplanar and they are glissile in nature. It is convenient in this case to associate each face of the tetrahedron with a certain junction group. Let us assume that it is possible for an incoming dislocation to react with two arms connected to the same junction node. Fig. A.17 (a) and (b) depicts this situation, where the black dislocation is about to react with two segments (arms), the orange and the green. If these

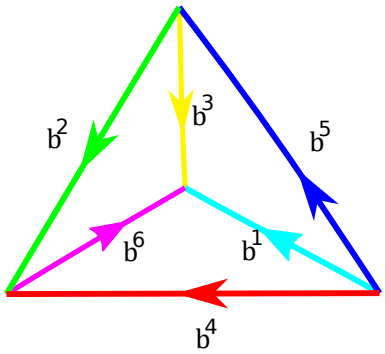

Figure A.16: Depiction of how the Burgers vectors in Table 1 are fixed on a tetrahedron, which is similar to the Thompson tetrahedron for FCC crystals.

reaction were possible, then the resulting graph would look like those in parts (c) and (d) in the figure, respectively. We have marked this reacting loop with the color black to signify that, at this moment, its Burgers vector can be any of the three Burgers vector group (blue, orange, green) shown in the figure. We now show that no matter what the Burgers vector chosen for the black loop is, a glissile junction cannot form when considering only one junction group (a triplet of Burgers vector). We note that the junction type (and thus group) of node v4 is the same as v3 (but opposite in orientation). The same can be said for nodes v5 and v6. In choosing a Burgers vector for the black segments, there are two options to choose from. The first is that both nodes v3 and v5 belong to the same junction group, and the second is that they do not. For the first option, if the black segment is to react with both the green and orange segments

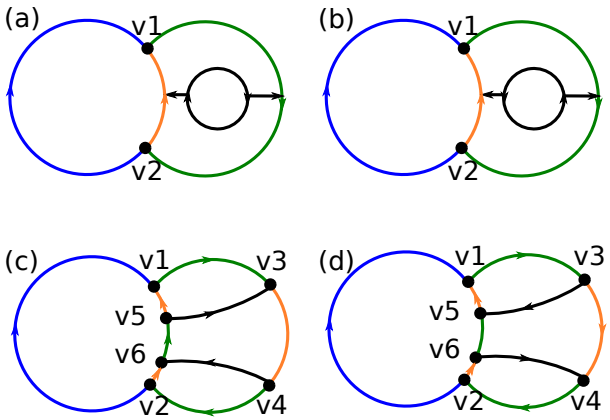

Figure A.17: A dislocation loop (black) is about to react with two arms (orange and green) connected to junction point v1. Two different reactions (a) and (b) are taking place to show how the orientation of the black segment affects the resulting graphs shown on the bottom.

(imagine picking two edges on the tetrahedron), then there is only one Burgers vector to chose from depending on what the Burgers vectors of the green and orange segments are (the last edge on the face which contains the previous two edges). With the coloring scheme provided in Fig. A.17 the black segment must be blue to have a chance to react with both segments. From the equation set in (A.1) we know that in each reaction two of the segments must be oriented similarly, and the third must be opposite. We note that the colors on the graph in Fig A.17 could correspond

to any set of three Burgers vectors given in (A.1). With this in mind, if we look at nodes v1,v3 and v5, we see that the set of segments that are oriented similarly change as we traverse from node to node in the graph, which is inconsistent with (A.1). We also note that this inconsistency is independent of how we fix the orientations of the Burgers vectors in Table 1. We can consider another scenario where we fix the burgers vectors such that $\boldsymbol{b}_1 + \boldsymbol{b}_2 + \boldsymbol{b}_3 = 0$, but there would still be inconsistency in this case due to the triangle that formed in the graph. We conclude that this first option, where nodes v3 and v5 have the same junction group, cannot produce junctions of one group.

Next, we address the second option where we allow the junction groups of nodes v3 and v5 to differ. In this case, it *is* possible for an incoming dislocation to react with two arms of the same junction node, but the bipartite property of the graph is destroyed. As mentioned in the main text, when multiple junction groups are considered, the graph is now r-partite, where r is 2n, and n is the number of junction groups. To remain a r-partite, the newly created junction nodes v3 and v5 must either all have different junction groups or be a mixture of different junction groups and orientations. It will be sufficient to show that whenever we have a triangle in the graph, like the one created by vertices v1,v3 and v5, we must have different junction groups for each of these vertices. This is because we are guaranteed differing orientations between v3 and v4 and also v5 and v6. To show that each node has a different junction group, we can use the closedness property of the total dislocation density tensor. If we draw a surface that encloses the triangle v1,v3, and v5, we can use the intersection property and the closedness property of the dislocation density tensor,

$$\int_{\partial V} \sum_{l=1}^{3} \boldsymbol{\alpha}_{\mathrm{s}}^{(l)} = 0. \tag{A.2}$$

This surface, ∂V, is depicted by the red line in the plane in Fig. A.18.

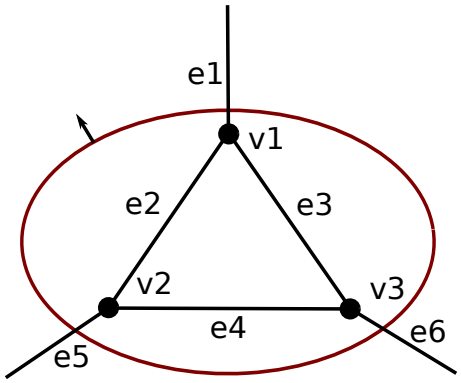

Figure A.18: A graphical representation of a dislocation network containing a triangle. This triangle is enclosed by a closed surface denoted by the red line.

From Fig. A.18 we learn that the segments e1, e5, and e6 must have Burgers vectors such that they could react with one another. We could for instance imagine that the Burgers vector of e1 was $\boldsymbol{b}_2$ then the edges e5 and e6 could either be $\boldsymbol{b}_6$ and $\boldsymbol{b}_3$ or $\boldsymbol{b}_5$ and $\boldsymbol{b}_4$. Whichever set is chosen for these edges ($\boldsymbol{b}_6$ and $\boldsymbol{b}_3$ or $\boldsymbol{b}_5$ and $\boldsymbol{b}_4$), it is important to note that the junction groups of the interior nodes v1, v2, and v3 cannot be part of the junction group which consist of the Burgers vectors for e1, e5, and e6. To show the latter, let e1, e2, and e3 be in this junction group by giving them

the Burgers vector $\boldsymbol{b}_2$, $\boldsymbol{b}_6$, and $\boldsymbol{b}_3$ respectively. In this case, e3 and e6 have the same Burgers vector and is not a valid junction type. If we now set e1, e2, and e3 to be $\boldsymbol{b}_2$, $\boldsymbol{b}_3$, and $\boldsymbol{b}_6$, respectively, then node v3 would also have to be in this group because the only reaction with both $\boldsymbol{b}_3$ and $\boldsymbol{b}_6$ is the junction group with $\boldsymbol{b}_2$,$\boldsymbol{b}_6$, and $\boldsymbol{b}_3$. Similar arguments hold for v2, and thus they have to all fall in the same group. We have shown earlier in this appendix that this is not allowed.

We refer to the choice of Burgers vectors for edges e1, e5, and e6 in Fig. A.18 as the 'face constraint', meaning that the remaining edges (e2,e3 and e4) in the same figure cannot form reactions with edges e1, e5, and e6 to give junction points (vertices) in the same junction group as that would result from the e1, e5, and e6 reaction. According to Fig. A.16 each Burgers vector may be involved in two junction groups corresponding to the faces that it is coincident with. This statement is valid for e1 which must form a reaction with e2 and e3 that is different from the reaction corresponding to the face constraint. Similarly edge e5 must form a reaction with e2 and e4 that is different than the reaction corresponding to the face constraint. Also e6 must form a reaction with e3 and e4 that is different than the reaction corresponding to the face constraint. Due to the geometry of the tetrahedron, the faces opposite of the constraint face are not the same, and thus the junction groups of the nodes v1,v2, and v3 are different. Interestingly, this results in the specification of a different Burgers vector for each of the six edges connected to the triangle.

Appendix B. Open line number density

In this appendix, we define a density variable associated with open dislocation lines, which represents the number density of dislocations ending or starting in a unit volume at a given point in space. Although this density is not used in our model equations, it is derived here for completeness. To obtain this density, we use a famous relation in graph theory called the degree sum formula (sometimes called the handshaking lemma), which takes on the form

$$|E| = \frac{1}{2}\sum_{v\in V}\deg(v), \tag{B.1}$$

where $|E|$ denotes the number of edges, deg is the number of edges connected to a vertex $v \in V$ with V denoting the vertex set of the graph. In this work, we argue for the use of positive and negative junction point densities, denoted by $\pi_{\mathrm{sJ}}^{+(p)}$ and $\pi_{\mathrm{sJ}}^{-(p)}$, respectively, to represent the junction nodes in the network. Since we are only considering junctions with 3 arms, the degree of each vertex is 3. From this information and (B.1), we define the open line number density E to be,

$$E = \frac{1}{2}\left[3\sum_{p\in S}(\pi_{\mathrm{sJ}}^{+(p)} + \pi_{\mathrm{sJ}}^{-(p)})\right] \tag{B.2}$$

where S is an index set containing all the junction types. We note that when we have information about the junction point densities we can obtain this measure at no additional cost. It is easy to see that this definition can be specialized to counting the number density of open lines belonging to a given slip system, ending or starting in a unit volume at a given point in space by considering only $\pi_{\mathrm{sJ}}^{+(p)}$ and $\pi_{\mathrm{sJ}}^{-(p)}$ for that slip system in the above expression. Such a density can be further defined for open dislocation lines involved in a particular junction group or junction type.

References

Sh. Akhondzadeh, Nicolas Bertin, Ryan B. Sills, and Wei Cai. Slip-free multiplication and complexity of dislocation networks in FCC metals. *Materials Theory*, 5(1):2, 12 2021. ISSN 2509-8012. doi: 10.1186/s41313-020-00024-y.

Joseph Pierre Anderson and Anter El-Azab. On the three-dimensional spatial correlations of curved dislocation systems. *Materials Theory*, 5(1): 1, 2021. ISSN 2509-8012. doi: 10.1186/s41313-020-00026-w.

Rajat Arora and Amit Acharya. Dislocation pattern formation in finite deformation crystal plasticity. *International Journal of Solids and Structures*, 184:114–135, 12 2020. ISSN 00207683. doi: 10.1016/j.ijsolstr.2019.02.013.

R Bott and L W Tu. *Differential forms in algebraic topology*, volume 82. Springer-Verlag New York, 1982. ISBN 978-0-387-90613-3. doi: 10.1007/978-1-4757-3951-0.

Vasily Bulatov and Wei Cai. *Computer Simulations of Dislocations*. Oxford University Press, 11 2006. ISBN 9780198526148. doi: 10.1093/oso/9780198526148.001.0001.

Vasily V. Bulatov, Luke L. Hsiung, Meijie Tang, Athanasios Arsenlis, Maria C. Bartelt, W Cai, Jeff N. Florando, Masato Hiratani, Moon Rhee, Gregg Hommes, Tim G. Pierce, and Tomas Diaz De La Rubia. Dislocation multi-junctions and strain hardening. *Nature*, 440(7088):1174–1178, 4 2006. ISSN 14764687. doi: 10.1038/nature04658.

Vincenzo Capasso. *An Introduction to Random Currents and Their Applications*. SpringerBriefs in Mathematics. Springer International Publishing, Cham, 2018. ISBN 978-3-319-94576-7. doi: 10.1007/978-3-319-94577-4.

Paolo Cermelli. Material symmetry and singularities in solids. *Proceedings of the Royal Society of London. Series A: Mathematical, Physical and Engineering Sciences*, 455(1981):299–322, 1 1999. ISSN 1364-5021. doi: 10.1098/rspa.1999.0314.

Georges de Rham. *Differentiable Manifolds*, volume 266 of *Grundlehren der mathematischen Wissenschaften*. Springer Berlin Heidelberg, Berlin, Heidelberg, 1984. ISBN 978-3-642-61754-6. doi: 10.1007/978-3-642-61752-2.

Jie Deng and Anter El-Azab. Dislocation pair correlations from dislocation dynamics simulations. *Journal of Computer-Aided Materials Design*, 14(S1):295–307, 12 2007. ISSN 0928-1045. doi: 10.1007/s10820-008-9090-4.

Reinhard Diestel. *Graph Theory*, volume 173 of *Graduate Texts in Mathematics*. Springer Berlin Heidelberg, Berlin, Heidelberg, 2 2017. ISBN 978-3-662-53621-6. doi: 10.1007/978-3-662-53622-3.

Marcelo Epstein and Reuven Segev. A unified geometric treatment of material defects. *arXiv: Mathematical Physics*, pages 1–14, 5 2013.

Marcelo Epstein and Reuven Segev. On the Geometry and Kinematics of Smoothly Distributed and Singular Defects. *arXiv: Mathematical Physics*, 2014.

Herbert Federer and Wendell H. Fleming. Normal and Integral Currents. *The Annals of Mathematics*, 72(3):458, 11 1960. ISSN 0003486X. doi: 10.2307/1970227.

I. Groma. Link between the microscopic and mesoscopic length-scale description of the collective behavior of dislocations. *Physical Review B*, 56 (10):5807–5813, 9 1997. ISSN 0163-1829. doi: 10.1103/PhysRevB.56.5807.

I Groma, F F Csikor, and Michael Zaiser. Spatial correlations and higher-order gradient terms in a continuum description of dislocation dynamics. *Acta Materialia*, 51:1271–1281, 2003. ISSN 13596454. doi: 10.1016/S1359-6454(02)00517-7.

Victor Guillemin and Peter Haine. *Differential Forms*. WORLD SCIENTIFIC, 6 2018. ISBN 978-981-327-277-4. doi: doi:10.1142/11058.

Victor Guillemin and Alan Pollack. Oriented intersection theory. In *Differential Topology*, pages 94–150. American Mathematical Society, Providence, Rhode Island, 8 2010. doi: 10.1090/chel/370/03.

J. P. Hirth, J. Lothe, and T. Mura. Theory of Dislocations (2nd ed.). *Journal of Applied Mechanics*, 50(2):476–477, 6 1983. ISSN 0021-8936. doi: 10.1115/1.3167075.

T. Hochrainer. *Evolving systems of curved dislocations:mathematical foundations of a statistical theory*. PhD thesis, Karlsruhe Institute of Technology, 2007.

T. Hochrainer. Multipole expansion of continuum dislocations dynamics in terms of alignment tensors. *Philosophical Magazine*, 95(12):1321–1367, 2015. ISSN 14786443. doi: 10.1080/14786435.2015.1026297.

T. Hochrainer, Michael Zaiser, and P. Gumbsch. A three-dimensional continuum theory of dislocation systems: kinematics and mean-field formulation. *Philosophical Magazine*, 87(8-9):1261–1282, 3 2007. ISSN 1478-6435. doi: 10.1080/14786430600930218.

T. Hochrainer, P Gumbsch, and M Zaiser. A Non-Linear Multiple Slip Theory in Continuum Dislocation Dynamics. In *Proceedings of the 4th Int. Conf. on Multiscale Materials Modelling*, pages 115–118, 2008. ISBN 978-0-615-24781-6.

Thomas Hochrainer. Thermodynamically consistent continuum dislocation dynamics. *Journal of the Mechanics and Physics of Solids*, 88:12–22, 3 2016. ISSN 00225096. doi: 10.1016/j.jmps.2015.12.015.

Chuanshi Hong, Xiaoxu Huang, and Grethe Winther. Dislocation content of geometrically necessary boundaries aligned with slip planes in rolled aluminium. *Philosophical Magazine*, 93(23):3118–3141, 8 2013. ISSN 1478-6435. doi: 10.1080/14786435.2013.805270.

Péter Dusán Ispánovity, Stefanos Papanikolaou, and I Groma. Emergence and role of dipolar dislocation patterns in discrete and continuum formulations of plasticity. *Physical Review B*, 101(2), 2020. ISSN 24699969. doi: 10.1103/PhysRevB.101.024105.

Ekkehart Kröner. Benefits and shortcomings of the continuous theory of dislocations. *International Journal of Solids and Structures*, 38(6-7): 1115–1134, 2001. ISSN 00207683. doi: 10.1016/S0020-7683(00)00077-9.

Ladislas P. Kubin, Ronan Madec, and Benoit Devincre. Dislocation intersections and reactions in FCC and BCC crystals. In *Materials Research Society Symposium - Proceedings*, volume 779, pages 25–36. Materials Research Society, 2003. doi: 10.1557/proc-779-w1.6.

John M. Lee. *Introduction to Smooth Manifolds*. Springer New York, second edition, 2013. ISBN 9780387217529. doi: 10.1007/978-1-4419-9982-5_1.

Peng Lin and A. El-Azab. Implementation of annihilation and junction reactions in vector density-based continuum dislocation dynamics. *Modelling and Simulation in Materials Science and Engineering*, 28(4), 2020. ISSN 1361651X. doi: 10.1088/1361-651X/ab7d90.

R. Madec, B. Devincre, and L. P. Kubin. From Dislocation Junctions to Forest Hardening. *Physical Review Letters*, 89(25):255508, 12 2002. ISSN 0031-9007. doi: 10.1103/PhysRevLett.89.255508.

I. H. (Ib Henning) Madsen and Jørgen. Tornehave. *From calculus to cohomology: de Rham cohomology and characteristic classes*. Cambridge University Press, 1997. ISBN 9780521589567.

E. Martínez, J. Marian, A. Arsenlis, M. Victoria, and J. M. Perlado. Atomistically informed dislocation dynamics in fcc crystals. *Journal of the Mechanics and Physics of Solids*, 2008. ISSN 00225096. doi: 10.1016/j.jmps.2007.06.014.

Mehran Monavari and Michael Zaiser. Annihilation and sources in continuum dislocation dynamics. *Materials Theory*, 2(1):30, 12 2018. ISSN 2509-8012. doi: 10.1186/s41313-018-0010-z.

Elihu Olami and Raz Kupferman. Homogenization of edge-dislocations as a weak limit of de-Rham currents. *arXiv: Mathematical Physics*, 2018.

Barrett O'Neill. *Elementary Differential Geometry*. Elsevier, 2006. ISBN 9780120887354. doi: 10.1016/C2009-0-05241-6.

Giacomo Po, Mamdouh S. Mohamed, Tamer Crosby, Can Erel, A. El-Azab, and Nasr Ghoniem. Recent Progress in Discrete Dislocation Dynamics and Its Applications to Micro Plasticity. *Jom*, 66(10):2108–2120, 10 2014. ISSN 15431851. doi: 10.1007/s11837-014-1153-2.

D Rodney and R Phillips. Structure and Strength of Dislocation Junctions: An Atomic Level Analysis. *Physical Review Letters*, 82(8):1704–1707, 2 1999. ISSN 0031-9007. doi: 10.1103/PhysRevLett.82.1704.

E Schmid and W Boas. *Plasticity of Crystals: With Special Reference to Metals*. Chapman & Hall, 1968. ISBN 9780412091308.

V. B. Shenoy, R. V. Kukta, and R. Phillips. Mesoscopic analysis of structure and strength of dislocation junctions in fcc metals. *Physical Review Letters*, 84(7):1491–1494, 2 2000. ISSN 10797114. doi: 10.1103/PhysRevLett.84.1491.

Ryan B. Sills, William P. Kuykendall, Amin Aghaei, and Wei Cai. Fundamentals of Dislocation Dynamics Simulations. In *Springer Series in Materials Science*, volume 245, pages 53–87. Springer, 2016. doi: 10.1007/978-3-319-33480-6_2.

Ryan B. Sills, Nicolas Bertin, Amin Aghaei, and W Cai. Dislocation Networks and the Microstructural Origin of Strain Hardening. *Physical Review Letters*, 2018. ISSN 10797114. doi: 10.1103/PhysRevLett.121.085501.

Kyle Starkey, Grethe Winther, and Anter El-Azab. Theoretical development of continuum dislocation dynamics for finite-deformation crystal plasticity at the mesoscale. *Journal of the Mechanics and Physics of Solids*, 139:103926, 6 2020. ISSN 00225096. doi: 10.1016/j.jmps.2020.103926.

Markus Stricker and Daniel Weygand. Dislocation multiplication mechanisms - Glissile junctions and their role on the plastic deformation at the microscale. *Acta Materialia*, 99:130–139, 2015. ISSN 13596454. doi: 10.1016/j.actamat.2015.07.073.

Markus Stricker, Markus Sudmanns, Katrin Schulz, T. Hochrainer, and Daniel Weygand. Dislocation multiplication in stage II deformation of fcc multi-slip single crystals. *Journal of the Mechanics and Physics of Solids*, 119:319–333, 10 2018. ISSN 00225096. doi: 10.1016/j.jmps.2018.07.003.

Markus Sudmanns, Markus Stricker, Daniel Weygand, T. Hochrainer, and Katrin Schulz. Dislocation multiplication by cross-slip and glissile reaction in a dislocation based continuum formulation of crystal plasticity. *Journal of the Mechanics and Physics of Solids*, 132:103695, 11 2019. ISSN 00225096. doi: 10.1016/j.jmps.2019.103695.

Markus Sudmanns, Jakob Bach, Daniel Weygand, and Katrin Schulz. Data-driven exploration and continuum modeling of dislocation networks. *Modelling and Simulation in Materials Science and Engineering*, 2020. ISSN 1361651X. doi: 10.1088/1361-651X/ab97ef.

Vignesh Vivekanandan, Peng Lin, Grethe Winther, and Anter El-Azab. On the implementation of dislocation reactions in continuum dislocation dynamics modeling of mesoscale plasticity. *Journal of the Mechanics and Physics of Solids*, 149:104327, 4 2021. ISSN 00225096. doi: 10.1016/j.jmps.2021.104327.

Benedikt Weger and Thomas Hochrainer. Leaving the Slip System - Cross Slip in Continuum Dislocation Dynamics. *PAMM*, 19(1), 11 2019. ISSN 1617-7061. doi: 10.1002/pamm.201900441.

Benedikt Weger, Satyapriya Gupta, and Thomas Hochrainer. Analysing discrete dislocation data using alignment and curvature tensors. *Comptes Rendus Physique*, 2021. ISSN 1631-0705. doi: 10.13140/RG.2.2.12288.15360.

Daniel Weygand and P. Gumbsch. Study of dislocation reactions and rearrangements under different loading conditions. *Materials Science and Engineering A*, 400-401(1-2 SUPPL.):158–161, 7 2005. ISSN 09215093. doi: 10.1016/j.msea.2005.03.102.

G. Winther, C.S. Hong, and X. Huang. Low-Energy Dislocation Structure (LEDS) character of dislocation boundaries aligned with slip planes in rolled aluminium. *Philosophical Magazine*, 95(13):1471–1489, 5 2015. ISSN 1478-6435. doi: 10.1080/14786435.2015.1033488.

Hussein M. Zbib, Tomas Díaz De La Rubia, Moono Rhee, and John P. Hirth. 3D dislocation dynamics: Stress-strain behavior and hardening mechanisms in fcc and bcc metals. *Journal of Nuclear Materials*, 276(1):154–165, 1 2000. ISSN 00223115. doi: 10.1016/S0022-3115(99)00175-0.